# Abstract

The imperative need to protect structures in mountainous areas against rockfall has led to the development of various protection methods. This study introduces a new type of rockfall protection fence made of posts, wire ropes, wire-netting and energy absorbers. The performance of this rock fence was verified in both experiments and dynamic finite element analysis. In collision tests, a reinforced-concrete block rolled down a natural slope and struck the rock fence at the end of the slope. A specialized system of measuring instruments was employed to accurately measure the acceleration of the block without cable connection. In particular, the performance of two types of energy absorber, which contribute also to preventing wire ropes from breaking, was investigated to determine the best energy absorber. In numerical simulation, a commercial finite element code having explicit dynamic capabilities was employed to create models of the two full-scale tests. To facilitate simulation, certain simplifying assumptions for mechanical data of each individual component of the rock fence and geometrical data of the model were adopted. Good agreement between numerical simulation and experimental data validated the numerical simulation. Furthermore, the results of numerical simulation helped highlight limitations of the testing method. The results of numerical simulation thus provide a deeper understanding of the structural behavior of individual components of the rock fence during rockfall impact.

In addition, a modified prototype is introduced as a developed prototype of the wire-rope fence. The cost-reducing modifications are increased post spacing and fewer wire netting layers. The numerical procedure again provides the nonlinear response of the prototype under various impact conditions and insights into each component's role in dissipating impact energy. Furthermore, a simple but effective method of increasing fence resistance is developed from analysis. Finally, the practical application of two units of the prototype to protect a wide area is investigated employing the numerical procedure.

# Acknowledgments

From the bottom of my heart, I would like to express my honest gratitude and high appreciation to my academic supervisor, Professor Koji Maegawa, for his continuous supports and kind encouragements, which strongly inspire me during the journey of doctoral course at Kanazawa University and successfully drive me to the end of the journey. The outstanding directions from him that I was guided at the every stage of my study will stand before me throughout my professional carrier in future.

I would like to extend my great thanks to Vietnamese government, Ministry of Education and Training for providing financial support during entire period of study.

Sincere appreciations are due to Raiteku Company. My study would not be completed without the enormous supports from the company for full-scale tests that are key portion in my study. I also wish to express my deepest gratitude to Kanazawa University as well as all members of Student Affair, who enthusiastically helped me since the beginning of my study and also the family life in Kanazawa.

I am extremely thankful to Mr. Yukio Abe and Mr. Mi Tetuo, who kindly helped me and my family since I started new life in Japan. I also would like to extend my special thanks to my dear friends and laboratory mates who assisted me directly or indirectly in both my study and daily life. For those I could not name them all, and for this purpose let me appreciate them.

I honestly express my deepest respect and extreme gratitude to my dear parents, brothers, sisters, beloved wife and my son for their patience, unconditional love, and support, strongly inspired me to accomplish my study.

# Contents

# List of Figures

# List of Tables

# Chapter 1 Introduction

## 1.1 General Background - Literature Review

### 1.1.1 Rockfall Phenomenon: Definition and Types of Rockfall

Rockfall is a rapid and rather spontaneous natural hazard that often occurs on steep slope, in which rock groups, or single rock blocks detached from the slope face fall down and maybe strike underlying infrastructures. This hazard often impacts to small region but its consequences are extremely severe, particularly to humanity. Rockfall differs from landslides by being distinctly extreme surface-phenomena; solid rock; regularly very small in volume; and mostly comprising of singular rather than massed units (Ladd 1935). And Ladd also subdivided rockfall into four types as follow: 1) Dribble of material; 2) Persistent fall of coarse material (often combined with fine), leading, in nature, to talus accumulations; 3) Falls of loosened rock from jointed or blast-shattered faces of cuts; and 4) Fall of single boulders, or a group of them, often of huge size, and sometimes from a great height (and long horizontal distance), loosened from rock outcrops or cliff faces by undermining as a result of weathering, rain, and seepage wash.

Another more encompassing definition of rockfall was proposed by Cruden and Varnes (Cruden et al., 1996), by which rockfall was defined as a very rapid to extremely speedy slope movement in which bedrock material is detached from a steep slope and descends the slope by falling, bouncing, or rolling. And Ritchie suggested the relationship between slope angle and the type of falling motion of rock blocks (Ritchie 1963). When the slope angle is more than $76^{o}$ (or 0.25:1), even the slight accelerative motion of rock blocks at their source can initiate a free fall. With the lesser steep slope, the falling rock hits the slope face and bounces, and when the slope angle is less than $45^{o}$, rolling motions dominate. Furthermore, relating to the rockfall volume, Rochet classified rockfall phenomena into four categories (Rochet 1987):

- Single block falls, which typically involve volumes ranging between 0.01 and 100 $m^3$.

- Mass falls, which typically involve volumes ranging between 100 and 100,000 $m^3$
- Very large mass falls, which typically involve volumes ranging between 100,000 and 10 million $m^3$.
- Mass displacements, which typically involve volumes greater than 10 million $m^3$

In general, rockfall hazard is recognized as a complex function of rock blocks of mass, velocity, rotation and jump height, strongly depend on slope characterization and rockfall mechanics (Broili 1973; Bozzolo et al., 1988; Azzoni et al., 1995)

### 1.1.2 Rockfall Causes

Rockfall is often triggered by a combination of internal and external causes. Internal causes can be the rock mass properties such as bedrock material type, discontinuity pattern, face topography, and ground water. External causes are triggering conditions that change the forces acting on a rock (Pantelidis 2009). They may be rainfall, snowmelt, seepage, channeled water runoff, weathering, erosion, freeze-thaw and heating-cooling cycles, tree roots, wind, disturbance by animals, and earthquakes. Additionally, human activities such as construction practices, blasting, vibration from equipment and trains, and stress relief due to excavation may be considered as external factors (Hoek 2007). Rockfall are often triggered by these external causes accompanied with rock mass instability.

McCauley surveyed 308 rockfall incidents along California highways and 14 causes of rockfall and their percentage of total were identified and displayed in Table 1 (McCauley et al., 1985). The table points out that causes related to the presence of water such as rainfall, freeze-thaw cycles, snowmelt, channeled runoff, and springs and seeps were totally counted for 67%. Rockfall records for a 19-year period on a major railroad in western Canada showed that approximately 70% of the events happened during the fall, winter, and spring with heavy rainfall, prolonged periods of freezing temperatures, and daily freeze-thaw cycles (Wyllie et al., 1996). Peckover did a statistic that rockfalls were most frequent on railway lines in the Fraser Canyon, British Columbia, Canada, between October and March, the wettest and coldest time of the year for the area (Peckover 1975).

153 slope failure events in Yosemite National Park were examined and triggering factors to each event are displayed in Table 2 (Guzzetti et al., 2003), in which 55% is counted for rockslides and 30% for rockfalls. Among triggering factors, water-related factors (rainfall, rainfall and snow, and freeze-thaw) took 73% of the failures and 14% was attributed to earthquakes.

Generally, there are many causes of rockfall, most of them relate to environmental factors. Particularly, the causes related to water are the most dominant factors triggering the rockfall events. And it is noted that rockfall only occurs as being triggered by combination of internal and external causes.

Table 1.1 Causes of 308 rockfalls on highways in California

| Causes of Rockfall | Percentage of Total |
|---|---|
| Rain | 30 |
| Freeze-thaw | 21 |
| Fractured rock | 12 |
| Wind | 12 |
| Snowmelt | 8 |
| Channeled runoff | 7 |
| Adverse planar fracture | 5 |
| Burrowing animals | 2 |
| Differential erosion | 1 |
| Tree roots | 0.6 |
| Springs or seeps | 0.6 |
| Wild animals | 0.3 |
| Truck vibrations | 0.3 |
| Soil decomposition | 0.3 |

Table 1.2 Triggering factors of slope failures in Yosemite National Park

| Triggering Factor | Number | Percentage |
|---|---|---|
| Rainfall | 78 | 51.0 |
| Rainfall and snow | 15 | 7.8 |
| Freeze-thaw | 18 | 11.8 |
| Earthquakes | 21 | 13.7 |
| Blasting and construction | 12 | 7.8 |
| Lightning, wind storms, spring runoff | 9 | 5.9 |

### 1.1.3 Setbacks of Rockfall Hazards

Compared to other disasters, rockfall usually affects only small region. However, the damage to the infrastructures, particularly transportations, or humanity may be highly serious with probable fatal consequences. Spang reported that rockfalls were the major cause of interruption to the West German Federal Railway's 28,000 km track network (Spang 1987). Martin concluded that rockfalls, small rockslides, and raveling are the most frequent slope stability problems along transportation routes in mountainous area of North America, annually required tens of millions of dollars on maintenance and protection measures to protect against such hazards (Martin 1988). Sasaki reported that Japan with 70% of mountains has suffered many slope disasters every year with several hundred lives lost (Sasaki et al., 2002)

Specifically, in 1977, large rockfall blocks closed Colorado State Highway 133 near Redstone, Colorado, for several days, pending their breakup by blasting and removal of material (Turner et al., 2012). On Monday, March 8, 2010, impacts of large rockfall blocks caused severe damage to the bridge deck located just west of Hanging Lake Tunnel in Interstate 70 in Glenwood Canyon, Colorado. Inter-state was closed from early Monday morning until Thursday afternoon while blocks were broken up by blasting and removed and while unstable residual rock block on slope was removed. Traffic lanes were restricted for extended period before bridge deck was repaired (Turner et al., 2012). Kariya reported a rockfall event in the Daisekkei Valley of Mount Shirouma-dake (1932 m), the northern

Japanese Alps that produced debris of ≥8000 m3, caused casualties of trekkers (Kariya et al., 2005). And Burlington Northern Santa Fe Railway train was hit by rockfall debris near Libby, Montana, on June 25, 2010. Sixteen cars derailed. Line was reopened one day later after emergency-response crews removed more than 5,400 m3 of debris from track (Turner et al., 2012).

### 1.1.4 Rockfall Basic Knowledge

Apparently, rockfalls are really considerable threat to lives, equipment, facilities, and transportation corridors in mountainous areas. Therefore, it is crucial to have the best protection based on rigorous hazard and risk management systems and a good understanding of the rockfall behavior as basic knowledge is necessary. They are site characters, rockfall mechanics, and rockfall trajectories.

The site characters include terrain characteristics, geological and geotechnical properties of earth materials, rock mass structure, groundwater conditions, and past and present geological processes. Investigation findings of site characterization enable develop a four-dimensional conceptual model, in which three spatial dimensions are combined with time as the fourth dimension to analyze the interactions of slope properties and processes (Turner et al., 2012). The conceptual model provides the basis to access the occurrence probabilities of rockfall hazard as well as analyze rockfall behavior, and ultimately helps determine proper mitigation procedures. If slope covers a limited area, conceptual geological model may be developed by reconnaissance study and forecast of rockfall behavior from back analysis of past events or by empirical methods. Other cases of slopes of large areas with frequent rockfall events, more detailed geological information, and slope topography are often required. Therefore, an extensive investigation of fieldwork and mapping and, probably, drilling to reach subsurface information are needed. There were many researches relating to this issue to identify the rockfall source zones, to determine the relatively susceptible geological materials in source zones to rockfall initiation, and to identify as well as describe the rockfall trajectories and run-out zones (Mazzoccola et al., 2000; Dorren 2003; Guzzetti et al., 2003; Coe et al., 2005)

Evaluation of rockfall mechanics is also required to deeply understand rockfall behavior. Mechanics of rock block movement are usually classified into four types: free falling, bouncing, rolling, and sliding. Among these types, bouncing and rolling that often appear after a falling block hit slope face are the most unknowable part of a rockfall travel path. Bouncing is typically described in a simplified approach using one or two coefficients of restitution (Wu 1985; Hungr et al., 1988; Pfeiffer et al., 1989; Azzoni et al., 1995). The free-fall trajectory is a parabola (Ritchie 1963). However, a rockfall movement may be any combination of above mechanics.

Rockfall prediction and modeling are often carried out to determine probable trajectories of rockfall blocks, their maximum run-out distance, and enabling estimate kinetic energy of the block. This information is really useful for the design of remedial measures of retaining fences and barriers, ditches and berms, or even rock sheds and tunnels. In addition, rockfall prediction and modeling, especially in combination with rock mass stability studies, become important components of hazard assessments for land use planning purpose, particularly in the populated mountainous regions (Turner et al., 2012). A typical serious workflow of a rockfall trajectory study at the scale of a community or a single slope can be divided into 6 phases: 1) preparation phase; 2) definition of the release scenarios; 3) rockfall modeling and simulation; 4) plausibility check/validation of the model results; 5) fixation of the model results; and 6) transformation into readable rockfall process maps (Lambert S. & Nicot F., 2011). So far available rockfall trajectory simulation models can be classified into 3 groups according to their spatial dimension: 1) two-dimensional (2-D) trajectory models; 2) 2.5-D or quasi-3-D trajectory models; and 3) 3-D trajectory models (Volkwein et al., 2011).

Over the past 30-year period, several 2-D rockfall simulation codes have been developed to anticipate rock block movements and significantly increase the knowledge and understanding of rockfall, allowing to specify relevant rockfall mitigation procedures (Cundall 1971; Cundall et al., 1979; Chen et al., 1999). The Colorado School of Mines supported by the Colorado Department of Transportation (DOT) as part of the rockfall hazard assessment efforts long the

Glenwood Canyon section developed the Colorado Rockfall Simulation Program (CRSP 1.0) in 1988-1989 to model rockfall behavior and provide statistical analysis of probable rockfall events at a given site (Pfeiffer et al., 1989; Pfeiffer et al., 1990). With the support of appropriate computer capacity, the newest version of CRSP extended in 3-D, termed CRSP-3D, was successfully developed to accurately model the motions of variably shaped rock block as they travel across slopes. However, whether a rockfall trajectory model is 2-D or 3-D, the experience in applying the model and knowledge of its sensitivity to parameter setting, as well as how to determine model parameter values in the field, is a prerequisite to obtain acceptable results (Volkwein et al., 2011)

### 1.1.5 Rockfall Mitigation

After properly obtaining basis information of rockfall probably happening on a specific slope, determination of a relevant mitigation measure is recognized as the most important step in hazard and risk management, i.e. a chosen corrective mitigation measure makes previous steps more meaningful.

In a corrective mitigation measure, the proper evaluation should focuses on multiple aspects of continuous maintenance, hazard lessening, and hazard removal. In addition, particular attention should be paid to the relationship between the annual maintenance costs and the reduction in the costs of potential consequences. For this reason, rockfall mitigation measures have been classified into two main groups: engineered and non-engineered. Engineered measures including three main categories of stabilization, protection, and avoidance are active interventions that diminish the occurrence of effects of rockfalls, while non-engineered measures are more passive interventions that include continued or increased maintenance, warning signs, and slope-monitoring systems (Turner et al., 2012)

Stabilization measures include changes in the slope to reduce occurrence probabilities of a rockfall. This can be done securing rocks in place, proactively removing loose rocks in a manageable manner, or improving the slope configuration to prevent rockfall internal causes from coming to triggering factors. Stabilization of rock slopes has been well documented in several publications (Fookes et al., 1976; Wyllie 1980; Wyllie et al., 1996; Schuster 1995; Morris et

al., 1999). Rock slope stabilization methods can be divided into two categories: rock reinforcement (Rock Bolting, Dowels, Shotcrete, Buttresses, Cable Lashing, Anchored Mesh, Cable Nets, Drainage) and rock removal (Scaling, Rock Removal, Blast Scaling, Trim Blasting, Resloping) (Turner et al., 2012).

Avoidance measures tend to relocate or realign transportations or other facilities away from zones with high probability of rockfall. Avoidance alternatives are often more costly than stabilization and protection alternatives. However, apparently they are safer than others. Particularly, avoidance alternatives become special attractive for large slopes with widespread sources of rockfall (Geiger et al., 1991).

Protection methods consisting of catchment areas, rigid barriers, flexible fences, drapery, and rockshed allow to control rockfalls when they initiate. The main goal of these types of approach is to alter the rockfall behavior by absorbing the falling energy or by capturing rockfalls to prevent them from hitting transportations or other vulnerable targets. This kind of method are more passive and warranted in conditions of (1) Rockfall source zones lie beyond the boundaries of the facilities; (2) The extent or nature of the source zone is impractical or excessively costly to stabilize; (3) Avoiding the hazard by facility relocation is not practical or excessively costly (Turner et al., 2012).

Barriers, such as embankments, earthen berms and structural walls, perform as rather rigid systems, capturing or deflecting falling rock blocks by their overall structural stiffness or huge mass. While draperies and fences functioning as flexible systems, dissipate the falling energy by their huge deformation when impact occur. Generally, protection alternatives are often more cost-effective than stabilization and avoidance ones. Simpler construction is required and fewer environmental impacts are warranted. However, they are not the solution of all situation of rockfall hazard.

### 1.1.6 Flexible Fences

Flexible fences are commonly employed to control or arrest falling rock blocks with the aim of protecting infrastructure. A flexible rockfall fence often consists of interceptive net, which directly intercepts falling rocks, and support structures

of posts anchored to foundations or to competent bedrock, tieback and lateral ropes, energy absorbing devices, and anchors. The net panel must have been able to provide huge deformation to dissipate the kinetic energy of falling rocks with significant support of accompanied energy absorbers. Compared with rigid barriers, flexible fences are often more cost-effective, and simpler in design. For these reasons, this kind of fence has been impressively developed for wide range of impact energy from 10 to 8000 kJ throughout the world.

Fences were initially applied to protection from snow avalanches in Switzerland; they involved triangular wire rope nets mounted on timber and, later, steel posts (Spang et al., 2001). Accidentally, this kind of fence was found to successfully capture rockfall that occurred during snow-free periods, opening its new application for rockfall protection since that time. The first known application of a wire rope fence for rockfall was erected in 1958 at Brusio on southern Switzerland for the protection of power transmission lines. The system consisted of individual rectangular nets measuring $3 \times 5$ m standing 5 m high, tall even by today's standards (Turner et al., 2012). During the past 50 years rockfall fence design involved a significant progress mainly based on increasingly modern apparatus for testing, innovation of computer science, and practical demand. Flexibility is consistently considered the basis of design; the enhancement only focuses on materials and constitutive components of the system. In modern fences, energy absorption capacity is the focal point of design. The intercept panel has been innovated using many new type of material from lightweight wire mesh to robust ring nets. In addition, several types of energy dissipation device have devised, leading to remarkable movement in the fence capacity against rockfall.

When a rockfall strike a fence, the impact energy is transferred from impact location into adjacent system components and immediately dissipated by the huge flexure of the fence panel along with the performance of any friction energy absorbing devices, if incorporated as part of the fence. Commonly it takes the fence 0.5 s to stop the rock block.

The evaluation of the fence performance is often based on the relationship between impact loading, maintenance, and efficiency (Turner et al., 2012). Impact loading is simply the kinetic energy that rockfall impact transfers to the fence.

Maintenance relates to required repairs from an impact. The effectiveness of the fence in distributing impact load while diminishing damage discloses the fence efficiency that is strongly influenced by impact location. The fence often reaches the peak of efficiency at the center of intercept panel, where fence panels can fully flex. Flexibility lessens the rockfall loads imparted to fence components and generally enhances the overall ability of the system to absorb greater impact energies with less maintenance. Flexibility and energy dissipation decrease as the impacts target toward the more rigid structures located away from the center point. Consequently, the increase of the maintenance cost of the fence system is certainty after hazard.

The advance in system performance and capacity that have been achieved over the past 50 years would not have been possible without extensive testing of fence systems and components, both in laboratory and from full-scale impacts. This is illustrated most impressively by the increase in fence capacities from an initial 50 kJ to about 8,000 kJ during the period, a nearly 100-fold increase in energy-absorption capacity (Spang et al., 2001)

The various individuals and groups from European countries, principally Switzerland and Italy, and Japan have conducted many full-scale tests on different kinds of rock fence to verify them and exchange information. Peila conducted field tests using a guide cable drive the weight from top the slope to targeted point on the fence located at slope base (Peila et al., 1998). The weight was loaded onto a trolley attached to the cable and traveled down slope to strike the fence without rolling and bouncing. In this manner, the impact energy was accurately calculated. Video cameras were used to monitor and record each test. The forces acting on the cables and posts were also measured.

Muraishi and Sano decribed the testing procedure used by the Japanese Railway Technical Research Institute (Muraishi et al., 1999). Verification of a fence was performed conducting laboratory-scale static strength tests on individual fence components as well as full-scale field test on the fence. The full-scale test was conducted by dropping a stone from crane into a test fence constructed on a steep slope. The fence plane created angle of $35^0$ from horizontal so that the angle between the fence and the rock trajectory was exactly $55^0$. With vertical drop test

the impact location and kinetic energy of the block can be reproduced identically in each of a series of tests, allowing reduce the number of required test to meet determined goal compared with the number of rock rolling tests conducted on a hill slope.

Baumann made a review of field tests on rock fences in Switzerland (Baumann 2002). There were more than 350 field tests performed in the country from 1988 to 2002, and the testing procedures as well as fence designs consecutively improved during the period. A summary of testing on flexible fence against rockfall is presented in (Thommen 2008). Then there were other full-scale tests with support of better measurement methods to obtain more detailed results (Gottardi et al., 2010). So far, based on how the falling block is accelerated, rockfall field tests can be grouped into two main categories: the test blocks are guided along inclined track cable and vertical free-falling.

In efforts to reduce number of costly full-scale tests but able to enable development of new types of rock fence, numerical simulation approaches have been performed for first entering deeply the responses of rock fences against rockfalls and then for designing or redesigning. Furthermore, numerical simulations allow consider special load cases that cannot be done in field tests (high-speed rockfall, multiple impact locations such as post/rope strike, etc.) as well as the response of the fence to its structural alterations (Fornaro et al., 1990; Nicot et al., 2001; Sasiharan et al., 2006; Volkwein, 2005; Cazzani et al., 2002). However, it is crucial that the numerical results should be validated by experimental results such as cable tension force, fence deformation as well as acceleration and the trajectory of the falling rock before using for design or redesign purposes.

## 1.2 Objectives and Scope of the Study

The main objective of this study is focus on rockfall protection with particular attention paid to developing of flexible fences. In this study, a new type of rock fence is shown to have a remarkable capacity to capture rocks and thereby prevent damage to transportations as well as fatalities. Basically, with regarding self-standing to make the fence more suitable to be installed along road side where

very little space exists, it was designed with an adequate stiffness without lateral guy cables and anchors. This basis makes the fence distinguishable from European styles.

This type of rock fence was scrutinized in both full-scale experiments and numerical simulation. In field tests, it has been the first time a reinforced-concrete (RC) block was actuated to roll down a natural slope and strike the fence erected at slope base without a navigation system. As a result, the effect of composite motion of an RC block (translation and rotation) on the performance of the rock fence will be clear. To support these tests, laboratory pre-tests on such components as energy absorbing devices and posts were conducted to examine their load-carrying capacities and structural behaviors. In addition, an experimental measure system was devised to control and obtain more detailed results from the tests.

Numerical simulation using the finite element code LS-DYNA reproduced the fence response against impact of the block, enabling to reach a deeper understanding of the structural non-linear behavior of the fence under severe dynamic condition. The valuable experimental data obtained from full-scale tests helped validate the numerical models in terms of the fence deformation, the block trajectory after impact, impact force between the block and the fence, etc. Parametric analysis with iterative execution was then performed to determine the structural function of each individual component of the system and how these components interact with one another during rockfall event. Furthermore, an investigation into the effect of the impact location on the resistance of the fence, which could not be done experimentally, was also carried out through a series of numerical models, allow verify the fence resistance under various impact conditions.

Based on gained understanding of this kind of fence, a new prototype is developed increasing post spacing and reducing the number of wire netting layer with the aim of reaching appreciable cost benefits. Above validated numerical procedure was employed to clarify the response of the prototype to these structural alterations before using in practice. Specifically, fence elongation, post deformation, and ultimately the energy absorption capacity of the developed prototype were thoroughly examined. Particularly, the response of side module (refer to

section 4.3.2 for details) of the prototype against rock impacts has been first time examined in the study, producing more detailed understanding about the fence resistance under various impact locations. Furthermore, to improve the fence resistance a simple but efficient enhancement method was proposed and scrutinized using iterative numerical models. Last but not least, this study also explored the performance of a fence comprising two units of the developed prototype, which is the most practical application suited to wide protection areas. And despite the numerical procedure specifically targeting the design of this fence, the methodologies and findings derived from this work are likely to be valuable to understanding comparable types of rock fence.

Following are Chapter 2 that presents experiments on a wire-rope rockfall protective fence, Chapter 3 expressing dynamic finite element analysis on the fence, and Chapter 4 set for introduction of a new prototype of the fence developed with three-dimensional numerical modeling.

## 1.3 References


Cazzani A., Mongiovì L., Frenex T. (2002). Dynamic Finite Element Analysis of Interceptive Devices for Falling Rocks. International Journal of Rock Mechanics and Mining Sciences 39(3): 303–321.

Azzoni A., Barbera G. L., A. Z. (1995). Analysis and Prediction of Rockfalls Using a Mathematical Model. International Journal of Rock Mechanics and Mining Sciences 32(7): 709–724.

Azzoni A., & De Freitas M. H. (1995). Experimentally Gained Parameters, Decisive for Rock Fall Analysis. Rock Mechanics and Rock Engineering 28(2): 111–124.

Baumann R. (2002). The Worldwide First Official Approval of Rock-Fall Protection Nets. The 53rd Annual Highway Geology Symposium, San Luis Obispo, Calif 40–51.

Bozzolo D., Pamini R., & Hutter K. (1988). Rockfall Analysis - a Mathematical Model and its Test With Field Data. The 5th International Symposium on Landslides, Balkema, Rotterdamm, Lausanne, Switzerland 555–563.

Broili L. (1973). In Situ Tests for the Study of Rockfall. Geologia Applicatae Idrogeologia 8:105-111.

Chen G., & Ohnishi Y. (1999). Slope Stability Analysis Using Discontinuous Deformation Analysis. The 37th U.S. Rock Mechanics Symposium, Rock Mechanics for Industry (B. Amadei, R. L. Kranz, and G. A. Scott, eds.), Vail, Colo., Balkema, Rotterdam, Nethrelands 535–541.

Coe J. A., Harp E. L., Tarr A. C., & Micheal J. A. (2005). Rock-Fall Hazard Assessment of Little Mill Campground, American Fork Canyon, Uinta National Forest, Utah. Open-file Report 2005-1229. U.S. Geological Survey, Reston, Va.

Cruden D.M., & Varnes D.J. (1996). Landslide Types and Processes. Special Report 247: Lanslide: Investigation and Mitigation (A.K. Turner and R.L. Schuster, eds.), Transportation Research Board, National Research Council, Washington, D.C. 36–75.

Cundall P. A. (1971). A Computer Model for Simulating Progressive, Large-Scale Movements in Blocky Rock Systems. Symposium on Rock Fracture of the International Society of Rock Mechanics, Nancy, France, Balkema, Rotterdam, Netherlands 2–8.

Cundall P. A., & Strack O. D. L. (1979). A Discrete Numerical Model for Granular Assemblies. Geotechnique 29: 47–65.

Dorren L. K. A. (2003). A Review of Rockfall Mechanics and Modeling Approaches. Progress in Physical Geography 27: 69–87.

Fookes P. G., & Sweeney M. (1976). Stabilization and Control of Local Rock Falls and Degrading Rock Slopes. Quarterly Journal of Engineering Geology 9: 37–55.

Fornaro M., Peila D., & Nebbia M. (1990). Block Falls on Rock Slopes-Application of a Numerical Simulation Programm to some Real Cases. The 6th International Congress IAEG, Rotterdam, Netherlands.

Geiger G., Humphries R. W., & Ingraham P. C. (1991). Design of Repairs to Highway Rock Slopes along the Ohio River in Ohio. National Symposium on Highway and Railroad Slope Maintenance, Association of Engineering Geologists, Denver, Colorado 75–90.

Gottardi, G., & Govoni, L. (2010). Full-scale Modelling of Falling Rock Protection Barriers. Rock Mechanics and Rock Engineering 43(3): 261–274. doi:10.1007/s00603-009-0046-0.

Guzzetti F., Crosta G., Detti R., & Agliardi F. (2003). STONE: A Computer Program for the Three-Dimensional Simulation of Rock Falls. Computers & Geosciences 28(9): 1079–1093.

Guzzetti F., Reichenbach P., & Wieczorek G. F. (2003). Rockfall Hazard and Risk Assessment in the Yosemite Valley, California, USA. Natural Hazards and Earth System Science 3(6): 491–503.

Hoek E. (2007). Practical Rock Engineering. Rocscience Inc., Toronto, Ontario, Canada. Retrieved from http://www.rocscience.com/education/hoeks_corner.

Hungr O., & Evans S. G. (1988). Engineering Evaluation of Fragmental Rockfall Hazards. 5th International Symposium on Landslides (C. Bonnard, ed.), Balkema, Rotterdam, Netherlands 1: 685–690.

Kariya Y., Sato G., Mokudai K., Komori J., Ishii M., Nishii R., Miyazawa Y., Tsumura N. (2007). Rockfall Hazard in the Daisekkei Valley, the Northern Japanese Alps, on 11 August 2005. Landslides (4): 91-94.

Ladd G. E. (1935). Landslides, Subsidences and Rockfalls as Problems for the Railroad Engineer. 36th Annual Convention of the American Railway Engineering Association 1091–1162.

Lambert S., & Nicot F. (2011). Rockfall Engineering.

Martin D. C. (1988). Rockfall Control: an Update. Bulletin of the Association of Engineering Geologists XXV(1): 137–139.

Mazzoccola D., & Sciesa E. (2000). Implementation and Comparison of Different Methods for Rockfall Hazard Assessment in the Italian Alps. The 4th Congress of the International Association of Engineering Geologists (E. Bromhead, N. Dixon, and M. L. Ibsen, eds.)-Landslides in Research, Theory and Practice, New Delhi, India 221–228.

McCauley M. L., Works B. W., & Naramore S. A. (1985). Rockfall Mitigation. FHWA Report FHWA/CA/TL-85/12. Federal Highway Administration, U.S. Department of Transportation, Washington, D.C.

Morris A. J., & Wood D. F. (1999). Rock Slope Engineering and Management Process on the Canadian Pacific Railway. The 50th Annual Highway Geology Sympposium, Roanoke, Va. 264–275.

Muraishi H., & Sano S. (1999). Full-Scale Rockfall Test of Ring Net Barrier and Components. Semonar on Rockfall Tests and Standardization, Davos, Switzerland.

Nicot, F., Cambou, B., & Mazzoleni, G. (2001). Design of Rockfall Restraining Nets from a Discrete Element Modelling. Rock Mechanics and Rock Engineering 34(2): 99–118. doi:10.1007/s006030170017.

Pantelidis L. (2009). Rock Slope Stability Assessment Throught Rock Mass Classification Systems. Rock Mechanics and Mining Sciences 46: 315–325.

Peckover F. L. (1975). Treatment of Rock Falls on Railway Lines. American Railway Engineering Association Bulletin 653 471–503.

Peila, D., Pelizza, S., & Sassudelli, F. (1998). Evaluation of Behaviour of Rockfall Restraining Nets by Full Scale Tests. Rock Mechanics and Rock Engineering 31(1): 1–24. doi:10.1007/s006030050006.

Pfeiffer T. J, & Bowen T. (1989). Computer Simulation of Rock Falls. Association of Engineering Geologists Bulletin 26(1): 135–146.

Pfeiffer T. J., & Higgins J. D. (1990). Rockfall Hazard Analysi Using the Colorado Rockfall Simulation Program. In Transportation Research Record 1288, Transportation Research Board, National Research Council, Washington, D.C. 117–126.

Ritchie A. M. (1963). Evaluation of Rockfall and Its Control. In Highway Research Record 17, Stability of Rock Slopes, Highway Research Board, National Research Council, Washington, D.C. 13–28.

Rochet L. (1987). Application of Numerical Propagation Models to the Study of Rocky Lanslides. Bulletin Liaison des Ponts et Chaussées 150-151, 84–95.

Sasaki Y., Dobrev N., Wakizaka Y. (2002). The Detailed Hazard Map of Road Slopes in Japan. Public Works Research Institute, Japan.

Sasiharan, N., Muhunthan, B., Badger, T., Shu, S., & Carradine, D. (2006). Numerical analysis of the performance of wire mesh and cable net rockfall protection

systems. Engineering Geology 88(1-2): 121–132. doi:10.1016/j.enggeo.2006.09.005

Schuster R. L. (1995). Recent Advanaces in Slope Stabilization. The 6th International Symposium on Landslides, Balkema, Rotterdam, Netherlands 3: 1715–1745.

Spang R. M. (1987). Protection against Rockfall Stepchild in the Design of Rock Slopes. 6th International Conference on Rock Mechanics, Montreal, Quebec, Canada, Balkema, Rotterdam, Netherlands 551–557.

Spang R. M., & Bolliger R. (2001). From the Timber Fence to the High Energy Net: Developments in Rockfall Protection from the Origins to the Present. Geobrugg Jubilee Conference, Bad Ragaz, Switzerland.

Thommen R. A. (2008). Testing of Various Types of Rockfall Flexible Wire Rope Mitigation Barrier: an Overview of Testing to date. The 59th Highway Geology Symposium, Santa Fe.

Turner A. K., & Schuster R. L. (2012). Rockfall Characterization and Control.

Volkwein, A., Schellenberg, K., Labiouse, V., Agliardi, F., Berger, F., Bourrier, F., Dorren, L. K. A., et al. (2011). Rockfall characterisation and structural protection – a review. Natural Hazards and Earth System Science 11(9): 2617–2651. doi:10.5194/nhess-11-2617-2011.

Volkwein, A. (2005). Numerical Simulation of Flexible Rockfall Protection Systems. Computing in Civil Engineering 179: 122–122. doi:10.1061/40794(179)122.

Wu S. S. (1985). Rockfall Evaluation by Computer Simulation. Transportation Research Record 10311, Transportation Research Board, National Research Council, Washington, D.C. 1–5.

Wyllie D. C. (1980). Toppling Rock Slope Failures, Examples of Analysis and Stabilization. Rock Mechanics 13: 89–98.

Wyllie D. C., & Norish N. I. (1996). Stabilization of Rock Slopes. In Special Report 247: Landslides: Investigation and Mitigation (A. K. Turner and R. L. Schuster, eds.), Transportation Research Board, National Research Council, Washington, D.C. 474–504.

# Chapter 2 Experiments on a Wire-Rope Rockfall Protective Fence

## 2.1 Introduction

Many methods of protecting against rockfall have been devised around the world. They can be classified into prevention and protection types. A prevention method involves the removal or stabilization of dangerous rocks on a slope. A protection method uses interceptive structures such as an embankment, a rock shed or a rock fence to catch rockfall in the middle or at the end of a slope.

An embankment has the advantage of lower construction and repair costs and the capacity to absorb higher rockfall energy than other structures, but it requires a suitable construction site. The embankment approach has been experimentally and numerically analyzed (Ronco et al. 2009; Lambert et al. 2009; Maegawa et al. 2011).

Many rock sheds have been constructed for mountainous roads in Japan. Impact tests have been carried out on a real rock shed to confirm its ultimate capacity (Kishi et al. 2002). However, the design basis for a rock shed in the Rockfall Mitigation Handbook (Japan Road Association 2006) is allowable stress design and leads to underestimation of the performance–cost ratio of a rock shed compared with the other structures.

The principal advantages of a rock fence are its rapid erection and easy maintenance. Some countries such as Japan, Italy, Switzerland, France and the United States have developed many types of rock fence. For instance, different types of fence were tested at a field test site in Europe, and flexible and practicable solutions for designing and constructing a rock fence were established as guidelines for the approval of rockfall protection kits (Gerber 2001; ETAG-027 2008). A flexible rock fence made from polyethylene netting, which is resistant against alkalis, acids, water, sudden impact, low temperature, and ultraviolet rays and can withstand high rockfall energy, was developed in Japan (Maegawa 2006). Rock fences made from netting have the important feature of being able to absorb

rockfall energy through their flexibility, which is achieved by large displacement of the cable net and by energy-dissipating devices mounted on the connecting cables.

In this study, a new type of rock fence made of posts, wire ropes, wire netting, and energy absorbers is shown to have a remarkable capacity to catch rocks and thereby prevent damage to vehicles and houses as well as fatalities. Basically, with regarding self-standing and accordance with narrow spaces of the fence, it was designed with an adequate stiffness without lateral guy cables and anchors. Moreover in Japan, the design scheme for a rock fence is based on a desired energy-absorption capacity (Japan Road Association 2006). To absorb a large amount of energy, the wire rope of the rock fence is semi-fastened to a post using an energy-absorbing device (Maegawa et al. 1995) as shown in Fig. 2.1 in which and following figures the default unit of dimensions is millimeter. When pulled, the wire rope does not slip from the device until the magnitude of the friction force exceeds a critical value, which is possible to vary. As the wire rope slips, the device is able to maintain a fluctuating kinetic frictional force between it and the wire rope until a stopper located at the end of the rope comes into contact with the energy absorber. The wire rope thus does not break and part of the impact energy is absorbed by the energy absorber.

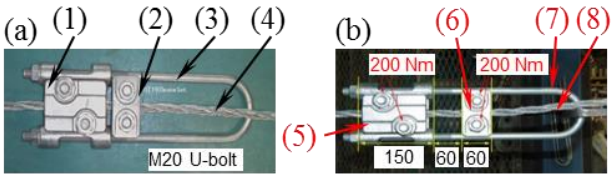


Figure 2.1 Absorber -Type A(a) and Absorber-Type B(b)

Two types of energy absorber will be introduced and examined with respect to their configuration and corresponding energy-dissipation behavior. To reduce the number of energy absorbers and achieve lower cost while maintaining perfor-

mance, energy absorbers were installed only at the end posts of the new type of fence. This type of rock fence was examined in full-scale experiments carried out using a reinforced-concrete (RC) block that rolled down a natural slope without a navigation system. Since an RC block under this experimental condition has not only translational motion but also rotational motion, the composite effect of the natural motion on the performance of the rock fence will be clear. In preparation for these tests, laboratory pre-tests on such components as energy absorbers and posts were conducted to confirm their load-carrying capacities and structural behaviors. Additionally, an experimental control system was devised to investigate the impact force between the block and fence in the tests.

## 2.2 Configuration of the Rock Fence

### 2.2.1 Details of the Rock Fence

Figure 2.2 shows the configuration and dimensions of the rock fence. Four posts made of concrete-filled steel tubes were vertically erected with a rigid joint on a concrete foundation, forming three spans with unequal length of 5, 8, and 5 m. These unequal dimensions come from the site condition that was just fit for the fence of 18 m long. Fortunately, it is certain that elongation of the 18 m long fence is smaller than that of equal length of 8, 8, and 8 m fence; i.e., likely safer to use the fence of 18 m in this study. Fourteen wire ropes employed as main components to catch rockfall were horizontally installed by connecting to both end posts via energy absorbers that are effective in preventing the wire ropes from breaking. Each wire rope passed a steel-ring welded to intermediate posts. The extension length of each wire rope from the energy absorber was 800 mm, and a stopper was attached at the end of each wire rope to prevent the rope from sliding out of the energy absorber. Additionally, seven vertical braces of steel plates were installed at mid-span of the fence to help maintain the spacing between wire ropes. The vertical brace semi-fastened each wire rope by two wire clips. With the aim of supporting the wire ropes to catch rockfall, two layers of wire netting comprising 5-mm steel wire having grid spacing of 50 mm were used. The wire netting and wire rope were connected by several steel-wire coils.

To brace the posts against one another in the plane of the fence, the top of each adjacent post was connected to a steel pipe functioning as a horizontal brace.

As shown in Fig. 2.1, two types of energy absorber were used in full-scale tests. The energy absorber consisted of a U-shaped bolt and two types of steel block. Each steel block consisted of two steel plates with thicknesses of 25 to 38 mm. The two steel plates were stacked one upon the other and the concave indentations of the two plates held in place a wire rope when they were compressed together by two M20 bolts at 200 Nm/bolt. The critical friction force between wire rope and the steel plates depends on the torque of the M20 bolts. Furthermore, as shown in Fig. 2.1a and b, the two types of energy absorber differ in the interval between the two steel blocks. In the Type-B energy absorber, the smaller steel block can initially slide along the U-bolt a distance of 60 mm, until contacting the larger one fixed to the U-bolt. In contrast, in the Type-A energy absorber, there is no interval between the two steel blocks and both of them are fixed to the U-bolt. This difference affects the timing of the maximum rope tension during rockfall collision.

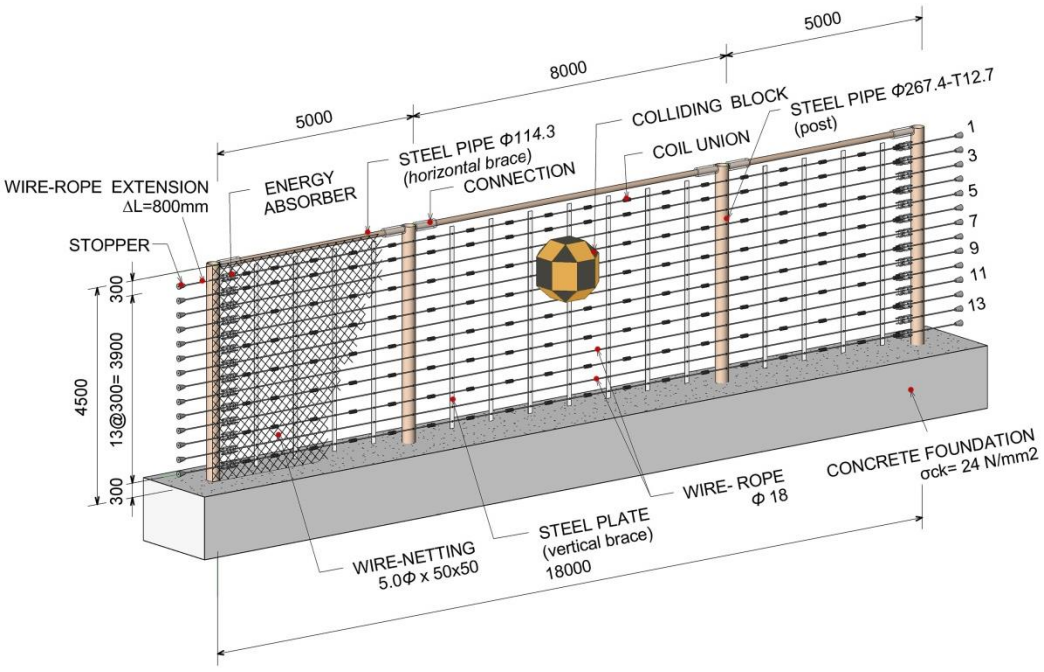


Figure 2.2 Configuration and dimensions of the rock fence (unit: mm)

### 2.2.2 Experimental Control System

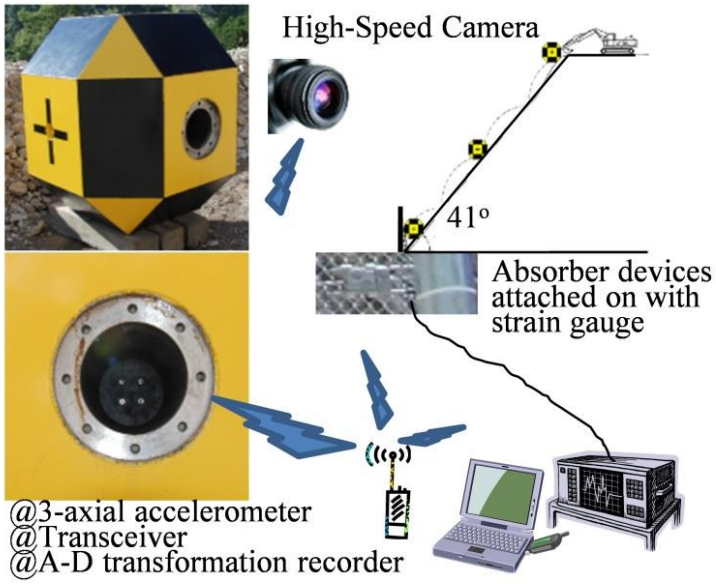


Figure 2.3 Experimental control system

Figure 2.3 shows the experimental control system mainly aimed at measuring the rope tension and the acceleration of the RC block. To record the acceleration data of the RC block at a sampling rate of 2 kHz, a three-axis accelerometer, analog-to-digital transformation recorder, and transceiver were placed at the center of the RC block. The transceiver acted to start up the recorder as soon as it received the trigger signal emitted from the master transceiver. Next, another analog-to-digital transformation recorder was synchronized to accumulate the data at a sampling rate of 2 kHz from strain gauges attached to the U-bolts of the energy absorbers. These data helped in estimating the wire-rope tension because the relation between the strain of the U-bolt and the tension force of the wire rope has been measured in a laboratory test. Additionally, a high-speed camera (600 frames/second) was set up on the side of the fence to capture the instant that the RC block makes impacts with the fence. Since the camera's starting frame was also synchronized, the frame number at the time of collision helped to specify the collision time in the acceleration history data. The RC block velocities were estimated from a series of frames shortly before the RC block strikes the fence. The prominent feature of this measurement system is that the accumulated data are synchronized by means of transceivers. Moreover, several other high-speed cam-

eras (300 frames/second) were set up at the most appropriate positions to monitor the interaction between the RC block and rock fence.

## 2.3 Outline of the Experiments

### 2.3.1 Pre-testing and Results for Energy Absorbers

Two types of energy absorber were tested in the laboratory to examine their behavior, in particular the friction force between the energy absorber and wire rope. Figure 2.4 describes the configuration and procedures of the laboratory test for an energy absorber. One end of the wire rope was connected to the test frame through a load cell, and the opposite part was held by an energy absorber; i.e., steel blocks. The outer wire rope from an energy absorber was free and was the extension for the sliding function. The remainder of the wire rope could be set at a length of about 5 m for the test, since the curved end of the U-bolt was connected to the test frame. The test procedure was as follows. A 1340-kg weight freely dropped along vertical guides and struck the middle of the wire rope, and the extension of the wire rope then slid through the energy absorber. The rope tension was measured using a load cell, and the rope slippage was calculated from the weight displacement measured using a rotary encoder connected to the weight. Additionally, the relation between the strain of each U-bolt used in the rock fence and the rope tension was examined in tensile tests under a static load. This relation was used to estimate the rope tension from the U-bolt's strain data recorded for the fence subjected to an impact load.

Figure 2.5 shows the results for the impulsive friction force for the two types of energy absorber. Independent of the device type, the impulsive friction force fluctuated widely, indicating that the wire rope exhibited alternate behaviors of slipping and stopping. However, the fluctuation of the Type-B energy absorber began at a lower friction force than that of the Type-A energy absorber. This difference certainly derives from the interval between the two steel blocks of the Type-B energy absorber, since the friction force initially occurred only in the larger steel block owing to this interval as mentioned in Section 2.2.1. No wire ropes broke during testing, and Fig. 2.6 shows that the maximum instantaneous friction forces for the Type-A and Type-B energy absorbers were 157 and 150

kN, respectively and they were less than the nominal strength of the wire rope (180 kN). Additionally, the average values of the impulsive friction force, obtained by dividing the final potential energy of the weight by the total slippage of the wire rope, were 65.2 and 45.4 kN for Type-A and Type-B energy absorbers, respectively.

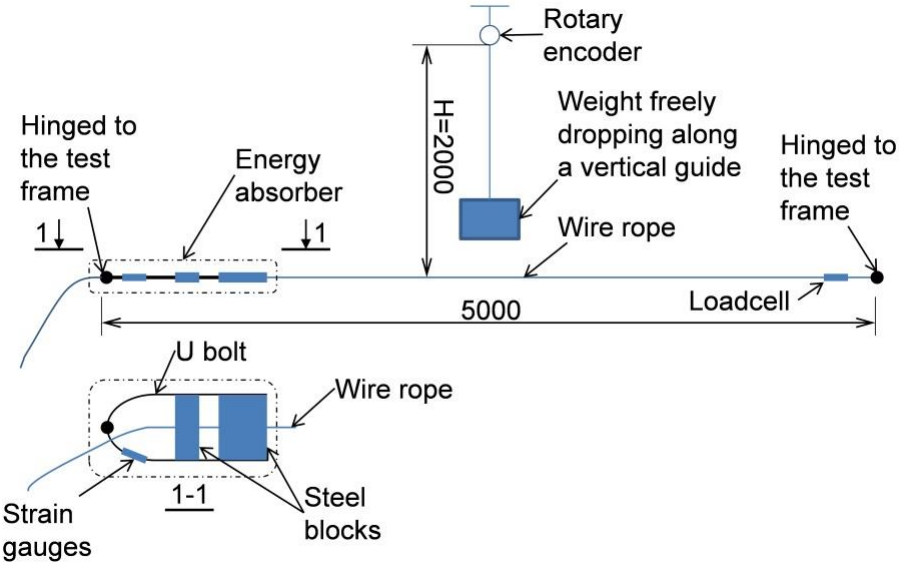


Figure 2.4 Laboratory test for an energy absorber (unit: mm)

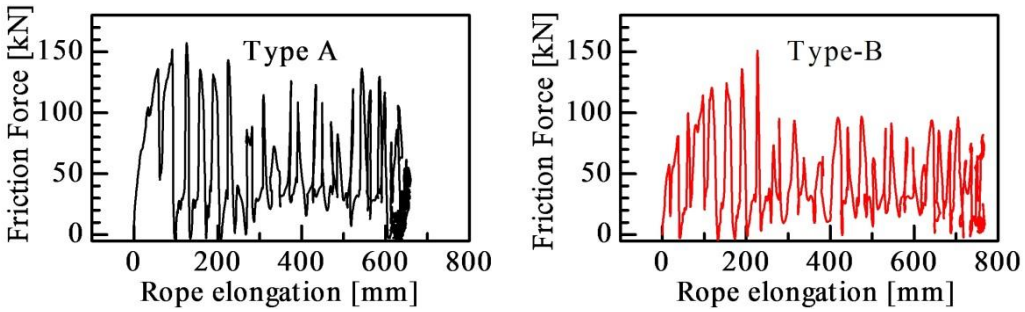


Figure 2.5 Impulsive friction vs. rope elongation curve

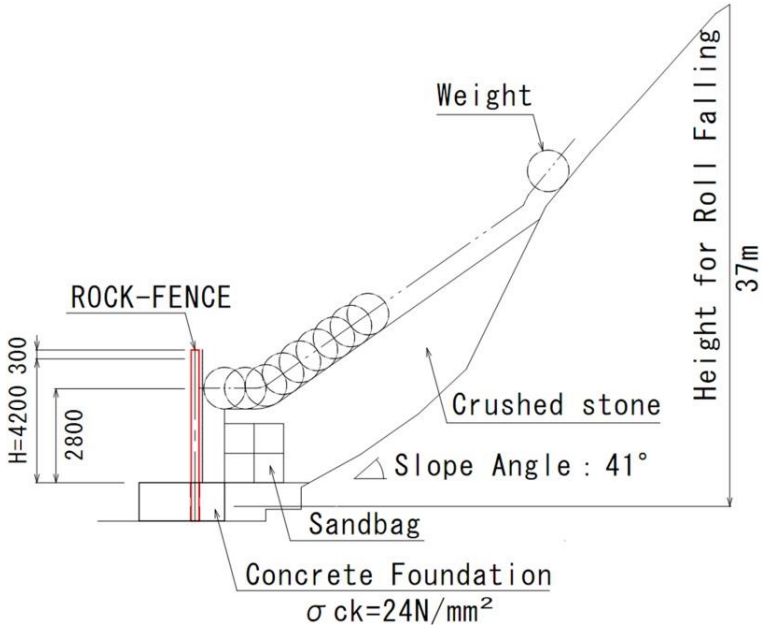


Figure 2.6 Test diagram

### 2.3.2 Test of the Rock Fence

Two tests were carried out. The sole difference between the tests is that Type-A and Type-B energy absorbers were applied in Tests No. 1 and No. 2, respectively. The mass of the weight and its falling height were identical in the two tests. After Test No. 1, all components other than the posts were replaced with new ones.

The shape of the RC block was in accordance with the EOTA guidelines for falling-rock protection kits (ETAG-027 2008), as shown in Fig. 2.3. The RC block was covered with 6-mm-thick steel plates and weighed 5.2 tons. In the tests, the block began rolling from the peak of a slope at a height of approximately 37 m and then stuck the fence, which was located at the bottom of the slope, as shown in Fig. 2.6.

## 2.4 Results of Rock Fence Tests

### 2.4.1 Behavior of the Rock Fence

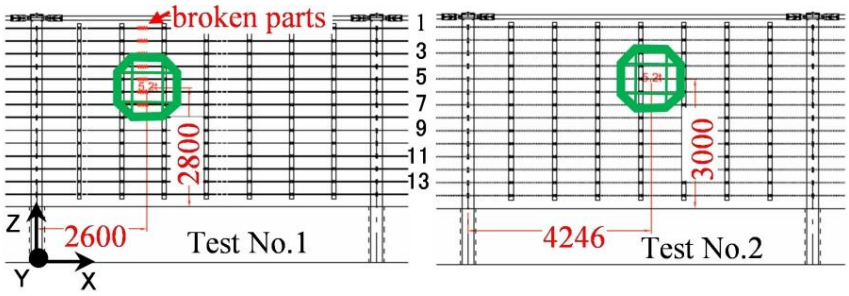


Figure 2.7 Collision point on the rock fence at mid-span

Figure 2.7 shows the collision point marked by an octagon at the mid-span of each fence. The collision point in Test No. 1 was slightly left of center. The target was set at a height of 2.7 m from the concrete foundation.

Figures 2.8 and 2.9 show the impact process; i.e., the motion of the RC block and the behavior of the rock fence just before and during the collision in Test No. 1 and Test No. 2, respectively, and the peak elongation of the wire netting. These images generally indicate that the fence could decelerate and captured the RC block in both tests. However, more thorough examination of the overall behavior of the fence shows differences between the two tests.

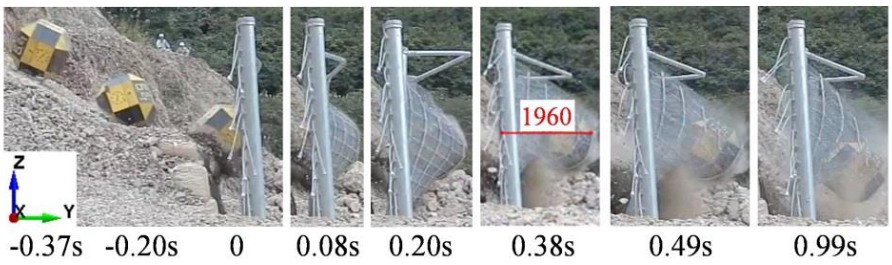


Figure 2.8 Behavior of the rock fence (Test No. 1)

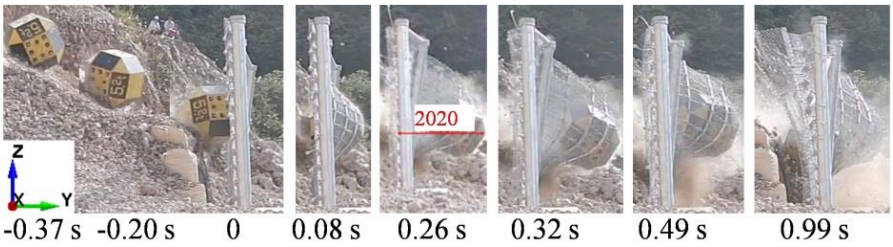


Figure 2.9 Behavior of the rock fence (Test No. 2)

Relating to the deformation of the fence, the peak elongation of the wire mesh in Test No. 2 was slightly larger than that in Test No. 1. Another discrepancy between two tests pertains to rope breaking. In Test No. 1, rope breaking was observed (wire ropes No. 1 through No. 7 broke, as shown in Fig. 2.7) and this is because the rope tension is not constant. It is higher in the impact region. In particular there was no slippage between the wire ropes and energy absorbers in Test No.1. In contrast, there was slipping in Test No.2 as illustrated in Fig. 2.10, enabling the fence to stop the RC block without the breaking of wire ropes.

After each test, theodolites were used to measure post deformation expressed by a post's declination in units of degrees in different directions with reference to the vertical. Site observations showed that the end posts only inclined in the fence plane and intermediate posts only inclined in a vertical plane perpendicular to the fence plane. Table 2.1 showing the declination data of the posts, shows that the deformation of the end posts in Test No. 1 was greater than that in Test No. 2, again demonstrating the great efficiency of the Type-B energy absorbers. Additionally, within each test, the collision location logically affects the difference in deformation between right and left posts.

Furthermore, the deformation of vertical braces in the Y-direction perpendicular to the fence plane, particularly the vertical braces in the impact region, generally reflecting the residual shape of the fence for both tests was measured. The maximum residual deformation in both tests is less than 1.1 m.

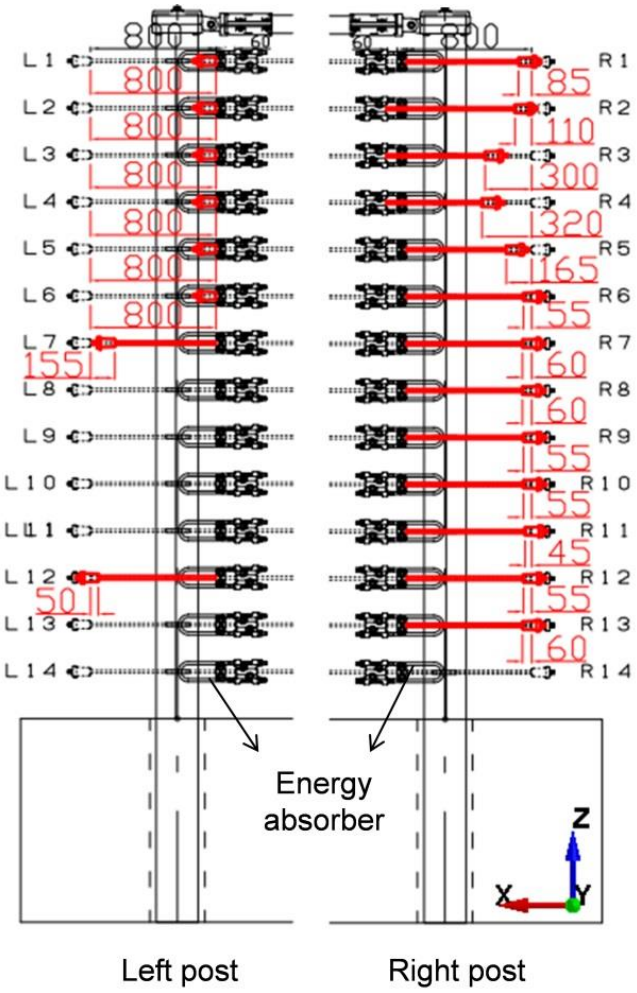


Figure 2.10 Wire rope slippage for Test No.2

Table 2.1 Deformation data for the posts in the two tests

| Posts | End posts | | Intermediate posts | |
|---|---|---|---|---|
| | Left | Right | Left | Right |
| Test No. 1 | 7.4$^{o}$ | 5.5$^{o}$ | 7.0$^{o}$ | 4.2$^{o}$ |
| Test No. 2 | 2.8$^{o}$ | 4.1$^{o}$ | 3.4$^{o}$ | 7.7$^{o}$ |

### 2.4.2 Impact Deceleration, Force, Velocity, and Energy

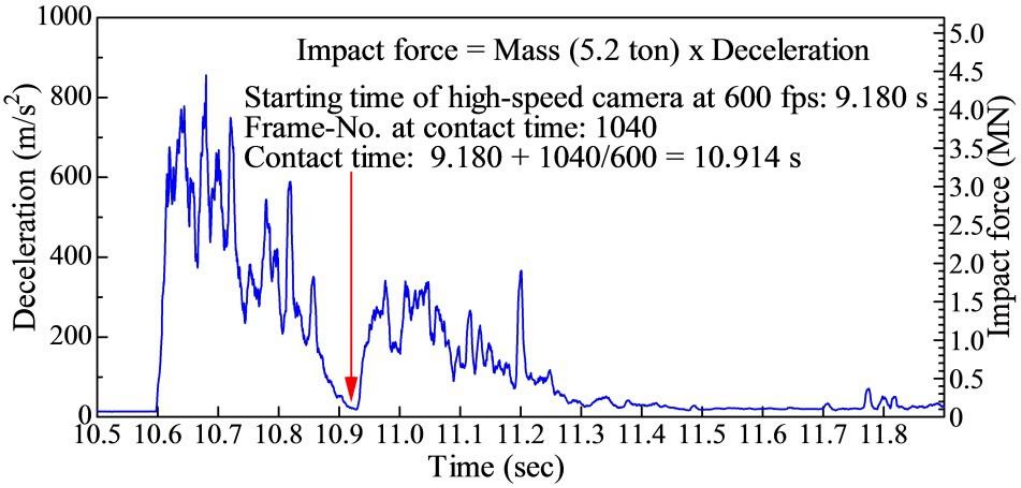


Figure 2.11 Deceleration and impact force history (Test No. 1)

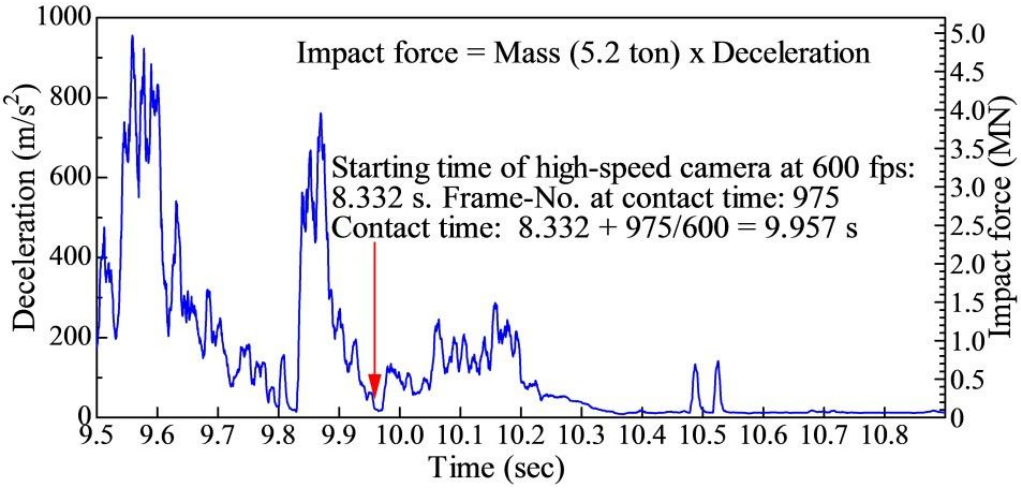


Figure 2.12 Deceleration and impact force history (Test No. 2)

Figures 2.11 and 2.12 show the resultant deceleration vs. time for Test No. 1 and Test No. 2, respectively, before and after collision. It is seen that the contact time can be estimated from the starting time of the high-speed camera and the frame number at which the RC block is observed striking the fence. Consequently, the deceleration and/or impact force due to the collision between the RC block and fence can be determined from the graph according to the contact time. The maximum deceleration and impact force were 280 to 340 m/s$^2$ and 1.46 to 1.77 MN, respectively. The deceleration (i.e., the impact force) in Test No. 1 was clearly

larger than that in Test No. 2. This result appears to be logically related to the fact that wire ropes No. 1 through No. 7 broke in Test No. 1.

According to the Japan Road Association Hand Book of Rockfall (Japan Road Association 2006), expected impact energy of approximately 1300 kJ was estimated for site conditions of slope of 41°, height of 37 m, and surface friction coefficient of 0.25. After the tests, however, the impact energy was recalculated from the block's impact velocities. The impact energy consists of translational energy ($E_v$) and rotational energy ($E_r$), which depend on the respective velocities of translation and rotation of the RC block just before collision:

$$E_v = MV^2/2, E_r = I\omega^2/2, \quad (1)$$

$$E = E_v + E_r, \quad (2)$$

where *M, I, V*, and ω are the mass, moment of inertia, translational velocity, and rotational velocity of the RC block, respectively. These component velocities of the RC block just before collision were approximately evaluated as follows. Before the tests, two separate points were firmly marked on the ground just in front of the fence at test site. The block's translational velocity was then calculated by dividing the distance between those points by the period of time that it took the block to pass through that distance and could be estimated from the number of frames of the block motion recorded by the high-speed cameras. The block's rotational velocity was determined solely from the recording of the block motion with the support of Videopoint software.

Table 2.2 Velocity and impact energy

| Test No. | Translation Velocity $V$ (m/s) | Rotation Velocity $\omega$ (rad/s) | Translation Energy $E_v$ (kJ) | Rotation Energy $E_r$ (kJ) | Total Energy $E$ (kJ) |
|---|---|---|---|---|---|
| 1 | 16.0 | 14.3 | 666 | 140 | 806 |
| 2 | 16.8 | 16.8 | 734 | 193 | 927 |

Table 2.2 gives the magnitudes of the translational and rotational velocities and the corresponding impact energies. The total impact energy was lower than the

expected energy. The reason for this may be that the RC block passed through a gravel layer placed in front of the rock fence to control the trajectory of the RC block because the layers of gravel were able to function as an energy-absorbing system (Pichler et al. 2005), and more importantly, the site surface friction coefficient used for the expected energy might be inappropriate. Table 2.2 indicates that the rotational energy was 17% to 20% of the total impact energy. This value might be larger than the expected value (Japan Road Association 2006), because the shape of the RC block used in this experiment rotates more easily than a rock during actual rockfall. Despite the larger rotational energy, the RC block did not bounce over the fence because of the flexibility of the fence structure.

## 2.5 Conclusion

This chapter presented experimental results for a newly developed rock fence able to vertically stand by itself without lateral guy cables and anchors. The fence was subjected to impact by an RC block rolling down a natural steep slope. The acceleration or impact force of the RC block colliding with the fence was measured with a measurement control system that was able to synchronize all measuring instruments. The impact energy approximately estimated in two full-scale tests (having different shock absorbers) was about 900 kJ, which is lower than that expected for the site conditions (Japan Road Association 2006). However, the rotational energy was 17% to 20% of the total impact energy, which is more than the value of 10% recommended by the Rockfall Mitigation Handbook (Japan Road Association 2006). Despite the higher rotational energy, the RC block did not bounce over the fence in either test because of the flexibility of the fence structure. More importantly, the residual deformation of the fence after impact was about 1000 mm, making the fence suitable to be installed just aside roads, where very little space exists.

Two types of energy absorber examined in laboratory pre-tests were assembled for the rock fences in the full-scale tests to confirm their energy-dissipation functions. The Type-B energy-absorbing device was found to be effective in preventing wire-rope breakage and in dissipating the impact energy of rockfall

and it thus considerably enhanced the impact energy absorption capacity of the fence.

As a final remark, it should be noted that experimental results obtained from full-scale tests provided a primary understanding of the overall performance of the fence against rockfall event, and in particular, they are necessary to validate adopted numerical models that are really useful for design or redesign purpose.

## 2.6 References


ETAG-027 (2008) Guideline for European Technical Approval of Falling Rock Protection Kits. European Organization for Technical Approvals (EOTA)

Japan Road Association (2006) Rockfall Mitigation Handbook.

Kishi N., Konno H., Ikeda K., Matsuoka K. G. (2002). Prototype impact tests on ultimate impact resistance of PC rock-sheds. International Journal of Impact Engineering 27: 969-985.

Lambert S., Gotteland P., Nicot F. (2009). Experimental Study of the Impact Response of Geocells as Components of Rockfall Protection Embankments. Natural Hazards and Earth System Sciences 9: 459-467.

Maegawa K. (2006). Weight impact tests on a flexible polyethylene net rock fence. Proc. of the 3rd International Conference on Protection of Structures against Hazards 43-50.

Maegawa K., Yoshida H (1995). Collision Tests on a New Type of Rock Barrier. Proceeding of EASEC-5 1927-1932.

Maegawa K., Yokota T., Tran P. V. (2011). Experiments on Rockfall Protection Embankments with Geogrids and Cushions. International Journal of Geomate 1(1): 19-24.

Pichler B., Hellmich C., Mang H. (2005). Impact of Rocks onto Gravel Design and Evaluation of Experiments. International Journal of Impact Engineering 31(5): 559-578. doi:10.1016/j.ijimpeng.2004.01.007.

Ronco C., Oggeri C., Peila D. (2009). Design of Reinforced Ground Embankments Used for Rockfall Protection. Natural Hazards and Earth System Sciences 9(1993): 1189-1199.

# Chapter 3 Dynamic Finite Element Analysis on a Wire-Rope Rockfall Protective Fence

## 3.1 Introduction

Although field-test is extremely important to reach the most real response of the flexible fence to rockfall, however it cannot provide diversified data of the fence's dynamic behavior under various impact conditions relating to impact location, structural changes. In particular, field test is often very costly. For these reasons, over the past years, many studies have focused on developing numerical procedures to accurately reproduce the fence response to rockfalls, allowing attain insights into performance of the fence as a whole system or each structural component of the system. After being thoroughly validated by experimental results obtained from field tests, numerical procedure becomes more trustable as a design tool.

This chapter presents a numerical procedure employed to reproduce two field tests on wire-rope rock fence as introduced in chapter 2 using the finite element code LS-DYNA. As mentioned above, first and foremost the numerical models were validated by comparing the results with those obtained in real-scale tests. The numerical simulation was then useful for parametric analysis. Iterative execution allowed us to examine the structural function of each individual component of the fence and how these components interact with one another during rockfall impact. Additionally, a series of numerical simulations was carried out to examine the effect of the impact location on the resistance of the fence, which could not be done experimentally, and to verify the rockfall energy absorption capacity of the fence under various impact conditions.

## 3.2 Finite Element Explicit Analysis

Because the impact phenomenon itself has a dynamic characteristic and involves large deformations, modeling the collision of an RC-block against a rock fence in numerical simulation based on a finite element method requires the consideration of nonlinear geometrical and mechanical behavior and particularly adequate contact conditions. For this reason, nonlinear dynamic analysis using LS-DYNA_971 is adopted to simulate the impact phenomenon in this study. With appropriate computational cost, this finite-element-method code can accurately analyze the rockfall impact, which lasts for only a very short period of a few seconds and involves rapid variations in force, velocity, acceleration, and contact condition.

## 3.3 Assumptions

The collision of the wire-rope rock fence subjected to rockfall can only be numerically simulated by making simplifying assumptions based on engineering judgment.

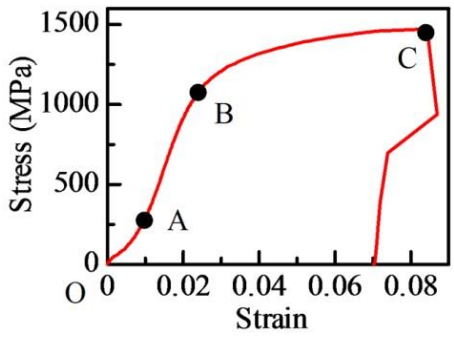


Figure 3.1 Stress–strain curve derived from the steel-cable static tensile test

First, the typical behavior of steel cable used as wire ropes in a standard static tensile test is depicted in Fig. 3.1. Another typical static tensile test carried out on pieces of steel wire used as wire netting was conducted to assert their load-carrying capacity.

In both cases, the authors are confronted with the problem of being unable to attain the dynamic material properties that should be obtained from dynamic tests. For simplicity and to retain only the most important observed characteristics of both wire rope, and wire netting, the author adopt a constitutive law that is bi-linear and rate-independent. This assumption might be disputed as being too rough an approximation. However, the effect of the strain rate phenomenon on the overall performance of the fence subjected to rockfall is not so considerable because of the low speed of rockfall impact as compared with that of a blast or a projectile and according to experimental tests. Grillo et al. (1985) pointed out that the assumption seems appropriate for steel members under impulsive loading. Thus, Figs. 3.2(a) and 3.2(b) show the assumed stress–strain curves for wire rope and wire netting, respectively, and the ultimate strength and the corresponding permanent strain are those deduced from static tensile tests with some appropriate engineering judgments.

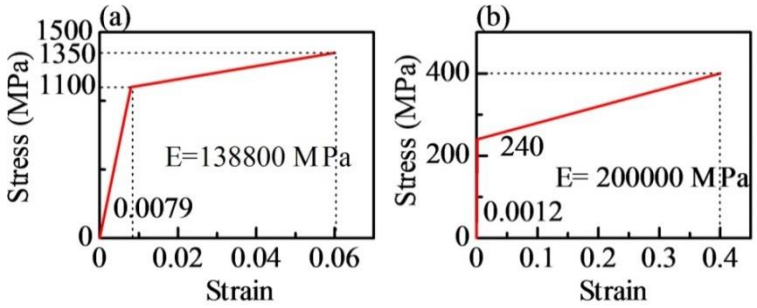


Figure 3.2 Assumed stress–strain curve applied for wire ropes (a); wire netting (b)

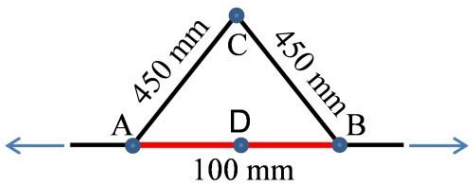


Figure 3.3 Numerical model applied for energy absorber

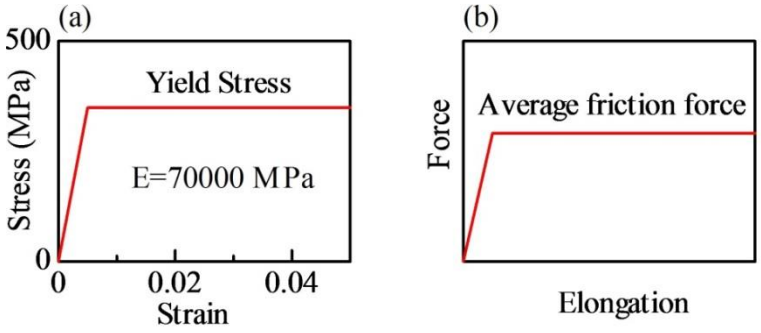


Figure 3.4 Assumed stress–strain curve (a); simplified behavior of absorbers (b)

Figure 3.3 shows the configuration of the numerical model representing energy absorbers. In this model, element AB with material properties complying with the stress–strain curve sketched in Fig. 3.4(a) is a key component. This element should express necessary structural functions that the real energy absorbers perform. Indeed, as shown in Fig. 3.4(b), after the yield stress point is reached, element AB begins lengthening under an invariable tension force, which is not an actual fluctuating friction force but is the average value of the impulsive friction force depending on the type of energy absorber. This behavior properly simulates the phenomenon of wire rope sliding through the energy absorber and therefore ensures that the absorbed impact energy in the numerical model is similar to that for the real fence. In addition, the presence of two elements AC and BC modeled as wire rope elements prevents the elongation of element AB from exceeding 800 mm, which is the peak slippage of wire ropes in Test No. 2. Indeed when points C and D coincide with each other, the length of element AB is approximately 900 mm; i.e., the elongation reaches a maximum of 800 mm.

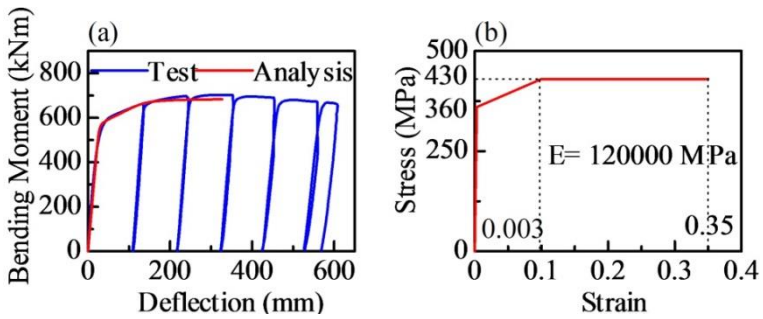


Figure 3.5 Bending moment vs. deflection curve of posts (a) and assumed stress–strain curve of posts (b)

The next important assumption is applied to the post constructed with a concrete-filled steel tube. LS-DYNA does not have appropriate composite material properties to model this type of component. A simplified model for the post was therefore made using a steel tube beam element with assurance that the load-carrying capacity and ductility of the post must be maintained. A three-point bending test on this post, which is supported by a span of 3.2 m, was carried out to determine the performance of the post; the bending moment vs. deflection curve is sketched as a blue line in Fig. 3.5(a). The beam of only a steel tube, which has the same outer diameter as the real post, was analyzed by searching for adequate values of thickness and Young's modulus. When the values of the thickness and Young's modulus were 30 mm and 120 GPa respectively, the red line obtained from analysis matched the blue line well, as shown in Fig. 3.5(a). From this result, the assumed stress–strain curve for the post modeled by only a steel tube is sketched in Fig. 3.5(b).

## 3.4 Numerical Simulation

The model used in the numerical simulation of the rock fence in Test No. 1 is referred to as Model No. 1 hereafter. Table 3.1 summarizes characteristics and parameters of Model No. 1. A cable element can be used to model wire rope or wire netting without consideration of the compressive force. However, because there is no definition of failure strain for the cable element in LS-DYNA, a truss element that can take a failure strain is adopted. Therefore, a pattern of alternate cable and truss elements are assigned to the wire rope and wire netting in the impact section to consider the possibility of breaking. To reduce the number of elements with the aim of reducing the execution time, the wire netting in Model No. 1 is simulated as just one layer of a 150 mm × 150 mm square grid. The wire diameter of the wire netting is therefore increased to 12.24 mm and the effective cross-sectional area is $A_{eff}$ = 117.63 $mm^2$, six times the original value. In fact, it was verified that there is no noticeable difference between the results analyzed using models having different grid sizes; i.e., 50 mm and 150 mm. The steel coil, which connects the wire rope and wire netting, is modeled by a K-element for

which the spring constant is $10^5$ N/m. The average friction force of 65 kN is applied for the energy absorber; i.e., Type A for Model No.1.

Furthermore, the consideration of the probable interaction of components within the fence during the impact is critical to achieving a good result. The automatic-contact definition used in Model No. 1 is based on the penalty method, which involves placing normal interface springs between all penetrating nodes and the contact surface. Table 3.2 presents the automatic contact definitions applied for components that probably interact with one another within Model No. 1.

Figure 3.6 illustrates the geometry of the wire-rope rock fence built in LS-DYNA, including the colliding block. Initially, the fence vertically stands in a plane and the trajectory of the colliding RC block lies in a vertical plane perpendicular to the fence plane. The block is modeled according to its real shape. According to EOTA guidelines (ETAG-027 2008), the volume of the block can be calculated as $V = 17/24 \times D^3$, where D is the maximum size of the RC block (1408 mm). Elastic-solid elements are assigned to the block with mass density of $2.63 \times 10^{-9}$ ton/mm$^3$, giving a weight of the block of 5.2 ton. The block is placed immediately next to the fence plane and assigned initial conditions of angular velocity $\omega$ = 14.3 rad/s, translational velocity in the Y direction (normal to the fence plane) $v_y$ = 15.8 m/s, and translational velocity in the Z direction $v_z$ = 2.3 m/s; these values were obtained from the results for Test No. 1.

Model No. 2 simulating Test No. 2 is similar to Model No. 1 on the whole, but the average friction force of 45 kN is applied for the energy absorber; i.e., Type B for Model No. 2. The initial conditions of the RC block are angular velocity $\omega$ = 16.8 rad/s, translational velocity in the Y-direction (normal to the fence plane) $v_y$ = 16.7 m/s, and translational velocity in the Z-direction $v_z$ = 2.3 m/s, which were obtained from the results in Test No. 2.

Table 3.1 Numerical data of Model No. 1

| Structural Component | Type of Element | Type of Material | Constitutive Law | Sectional Properties [mm] |
|---|---|---|---|---|
| Wire rope | a) Beam-Cable<br>b) Beam-Truss | a) Cable Discrete<br>b) Piecewise Linear Plasticity | Fig. 3.2a | ∅18 |
| Wire netting | a) Beam-Cable<br>b) Beam-Truss | a) Cable Discrete<br>b) Piecewise Linear Plasticity | Fig. 3.2b | ∅5 |
| Post | Beam | Piecewise Linear Plasticity | Fig. 3.5b | ∅267.4 × 30t |
| Horizontal Brace | Beam | Piecewise Linear Plasticity | Fig. 3.2b | ∅14.3 × 4.5t |
| Vertical Brace | Shell | Piecewise Linear Plasticity | Fig. 3.2b | 9t |
| Steel ring welded to post | Beam | Rigid | | ∅30 |
| U-bolts connected to vertical brace | Beam | Rigid | | ∅10 |

Table 3.2 Automatic contact definitions for Model No. 1

| Contact definitions | Components in contact |
|---|---|
| Automatic General | (wire rope vs. steel ring) ; (wire rope vs. vertical brace) ; (weight vs. vertical brace) |
| Automatic Nodes to Surface | (weight vs. wire netting) ; (weight vs. wire rope) |

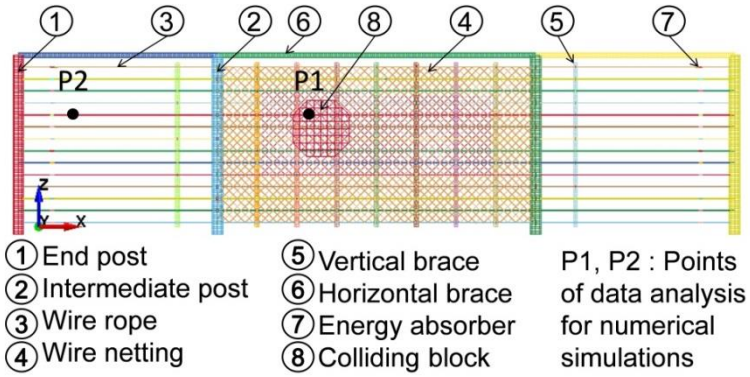


Figure 3.6 Technical sketch of the wire-rope rock fence built in LS-DYNA

## 3.5 Analysis, Validation and Discussion

### 3.5.1 Model No.1

Generally, the numerical behavior of the fence did not match well that of the real fence, with some of the wire ropes breaking in the latter case. Therefore, the best value of the average friction force was obtained by iterative execution in which the magnitude of friction was increased until a good result was achieved. Eventually, it was found that the model with an average friction force of 85 kN provided good results, as shown in Figs. 3.7 and 3.8, in which the fence was able to catch the block in spite of the breaking of wire ropes No. 6 and No. 7 and some damage to the wire netting. This numerical result matches the experimental result. Furthermore, Fig. 3.9 shows the Y-displacement of the central point of the impact area with time, and it is seen that the maximum displacement is close to that shown in Fig. 2.8 of Test No. 1 (Chapter 2).

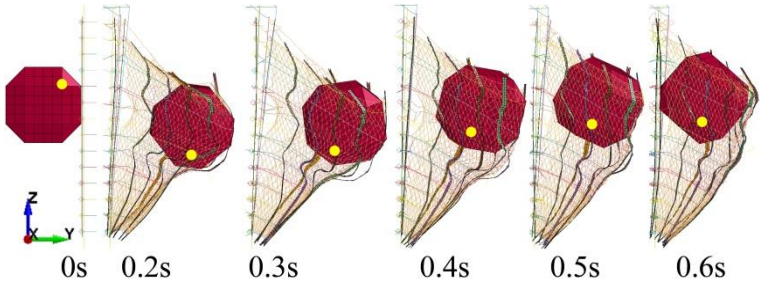


Figure 3.7 A series of motions in Model No.1

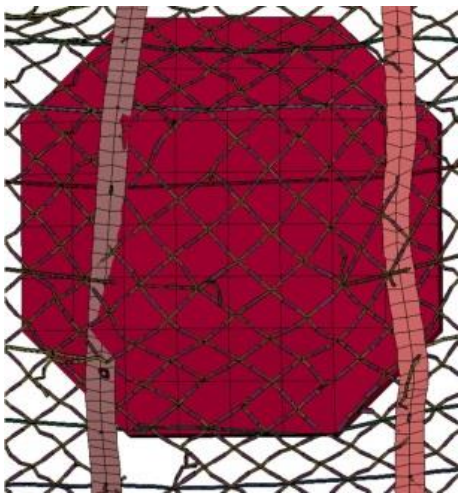

Figure 3.8 Damage to wire ropes No. 6 and No. 7 and wire netting

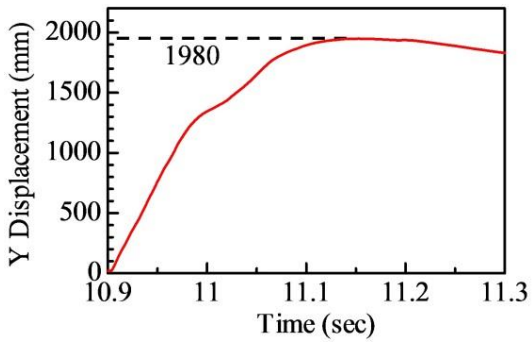


Figure 3.9 Time vs. Y-displacement of center of impact area in Model No. 1

It is thus asserted that numerical Model No. 1 can almost simulate Test No. 1 in terms of the overall behavior, the wire-rope breakage, and the deformation of posts, horizontal braces, and vertical braces. There is however a considerable difference between the test and the numerical model in terms of the number of broken wire ropes; i.e., 7 vs. 2.

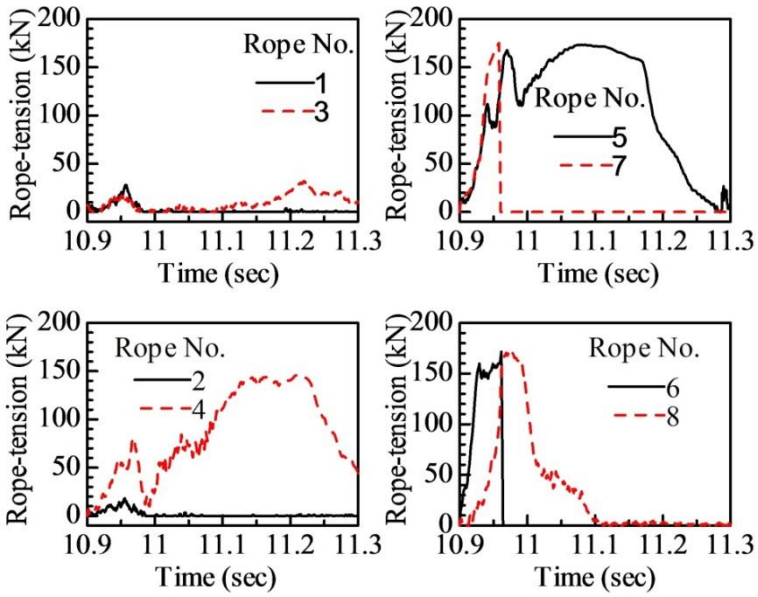


Figure 3.10 Time vs. Rope tension at impact section in Model No. 1

Figures 3.10 and 3.11 show the rope tension over time for each rope; the location of the ropes is indicated in Fig. 2.2 (Chapter 2). The figures present data calculated for the impact section and a section adjacent to an end post, respectively. It is clearly seen that rope Nos. 4 to 8, which passed through the contact area of the block and the fence, experienced greater tension in the impact section than in the section adjacent to the end post. However, the situation was the opposite for rope Nos. 1 to 3, which did not directly pass through the contact area. This phenomenon seems to come from the impact momentum being transferred from the contact area to the surrounding area via vertical braces and partly wire netting along a direction not perpendicular to the ropes.

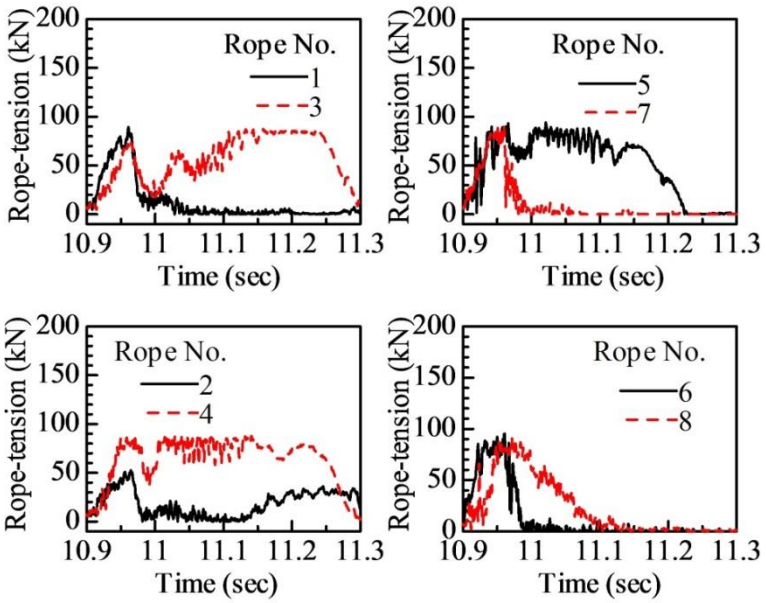


Figure 3.11 Time vs. Rope tension at section adjacent to an end post in Model No.1

Figure 3.12 shows the rope tension history measured in the section adjacent to the end post in Test No. 1. The method for measuring the rope tension from the strain at the U-bolt of an energy absorber is mentioned in Section 2.2 - Chapter 2. Although the peak values of tension for rope Nos. 1 to 7 were well under the tensile strength of 180 kN, all these ropes broke in the impact section in the test. According to the numerical results illustrated in Figs. 3.10 and 3.11, in the impact section in Test No. 1, the peak values of tension for rope Nos. 1 to 7 certainly reached the tensile strength and resulted in their breaking.

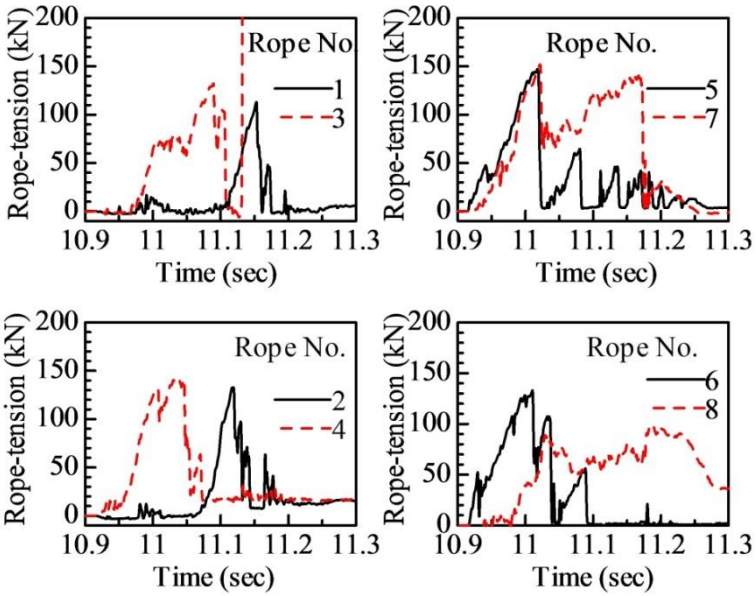


Figure 3.12 Time vs. Rope tension at section adjacent to an end post in Test No.1

### 3.5.2 Model No.2

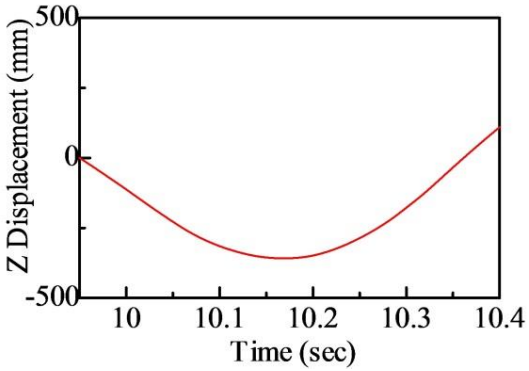


Figure 3.13 Time vs. Block movement in Z-direction in Model No. 2

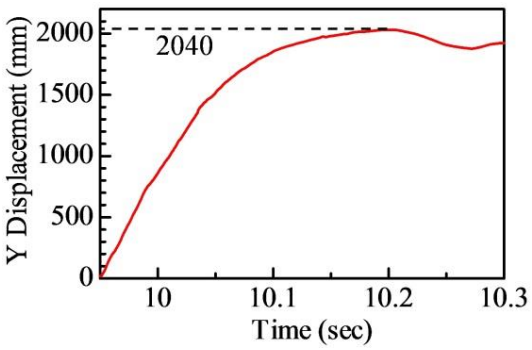


Figure 3.14 Y-displacement history of wire-mesh measured at center of contact area in Model No. 2

Owing to the flexibility of the fence and the effectiveness of the Type-B energy absorbers, the amount of dissipated impact energy increased considerably, resulted in no breakage of the wire ropes, only little damage to the wire netting, and great effectiveness in catching the RC block. In particular, there is good agreement between experiment and numerical simulation in terms of the general track of the RC block during collision and the deformation of the fence. In both simulation and experiment, the block rebounded after being stopped by the fence. Figure 3.13 depicts the movement history of the block's center in the Z-direction. Figure 3.14 shows the displacement history of the center of the contact area in the Y-direction. Figure 3.15 is the composite picture of an animation of Model No. 2. According to above points, it is obvious that the numerical simulation behavior of Model No. 2 agrees well with responses of the fence in Test No. 2.

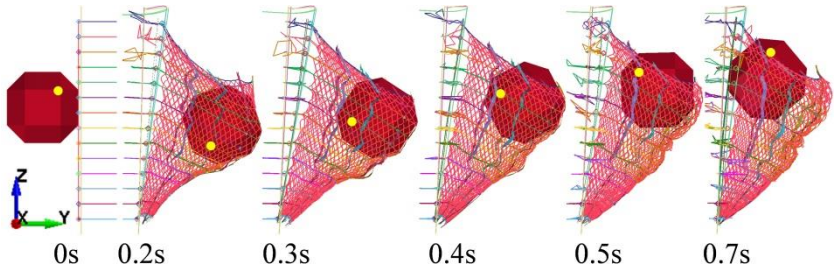


Figure 3.15 Composite picture from animation in Model No. 2

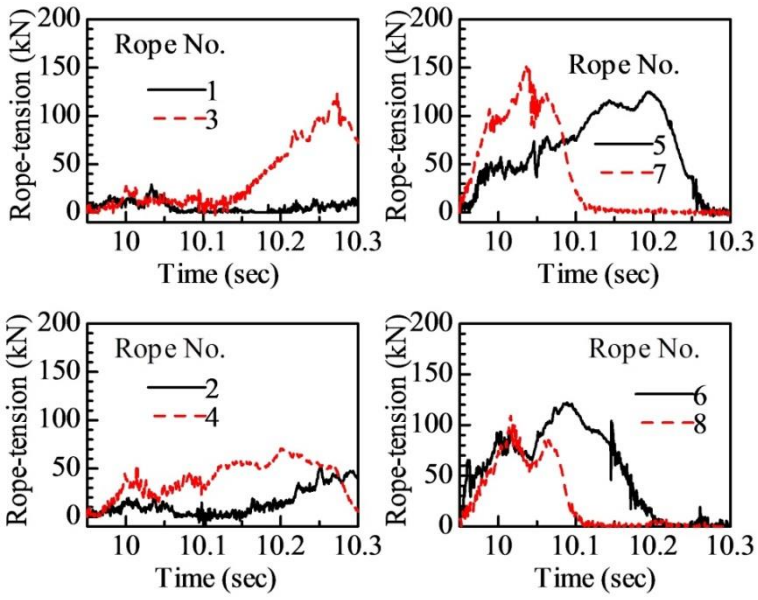


Figure 3.16 Time vs. Rope tension at impact section in Model No. 2

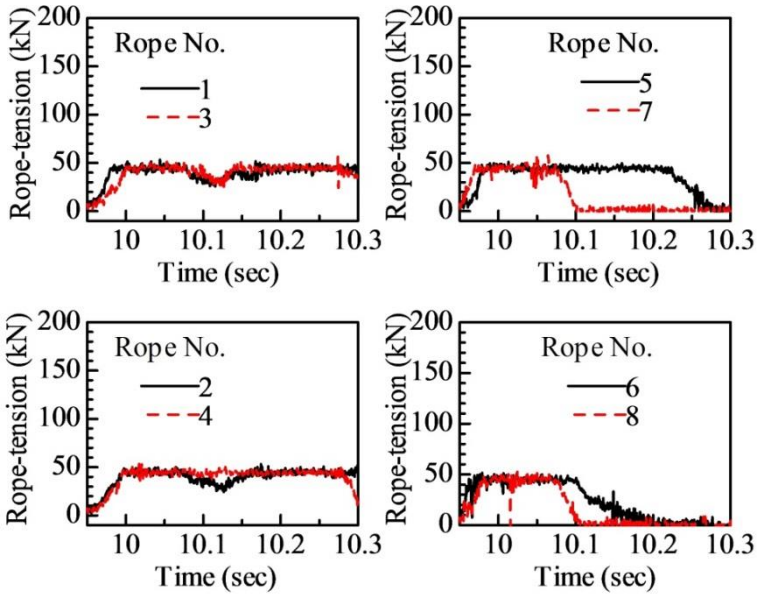


Figure 3.17 Time vs. Rope tension at section adjacent to an end post in Model No.2

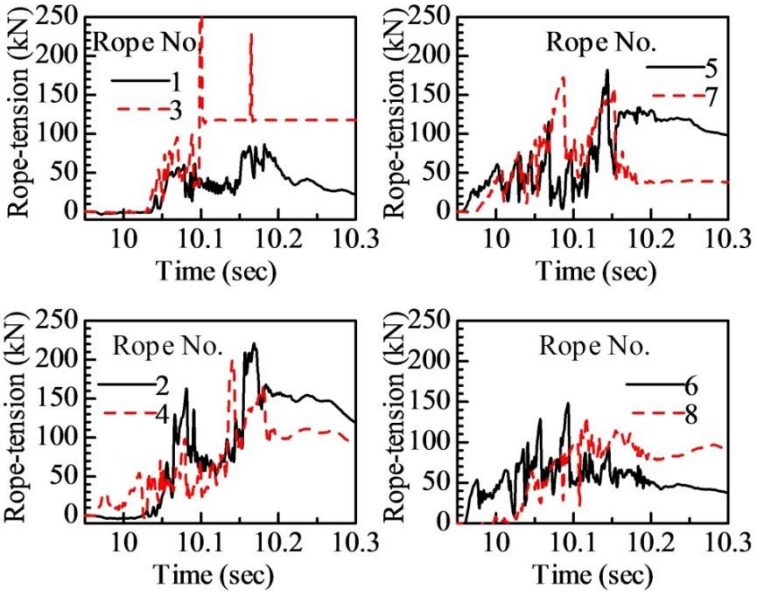


Figure 3.18 Time vs. Rope tension at section adjacent to an end post in Test No.2

Next, it is essential to analyze rope tension results for Model No. 2 and Test No. 2. There is a clear difference between Figs. 3.16 and 3.17, respectively showing the rope tensions calculated in the impact section and the section adjacent to the end post in Model No. 2; i.e., the rope tension was not constant along the rope

line and varied considerably and the reason of this phenomenon is going to discuss at the end part of this section. Figure 3.17 shows that the magnitude of rope tension remained constant at approximately 45 kN during the collision; i.e., the behavior of the energy absorber model was as prediction of the author in Section 3.3. Figure 3.18 illustrates the severe fluctuation of rope tensions in the section adjacent to the end post in Test No. 2, and tensions of rope Nos. 2 to 4 indeed seem to exceed the tensile strength of 180 kN but there was no breakage in Test No. 2. This discrepancy unfortunately arises from unreliable measurement of rope tensions using the mismatched cross-sectional size of U-bolts of absorbers, since real rope tensions probably exceeded the yield capacity of the U-bolt of 135 kN and therefore reached the region where the rope tension and U-bolt strain are not proportional. According to the experimental and numerical results, the energy absorber of Type B is functionally effective. Permitting wire rope to slide through a Type-B energy absorber not only dissipated the impact energy well but also prevented wire rope from breaking.

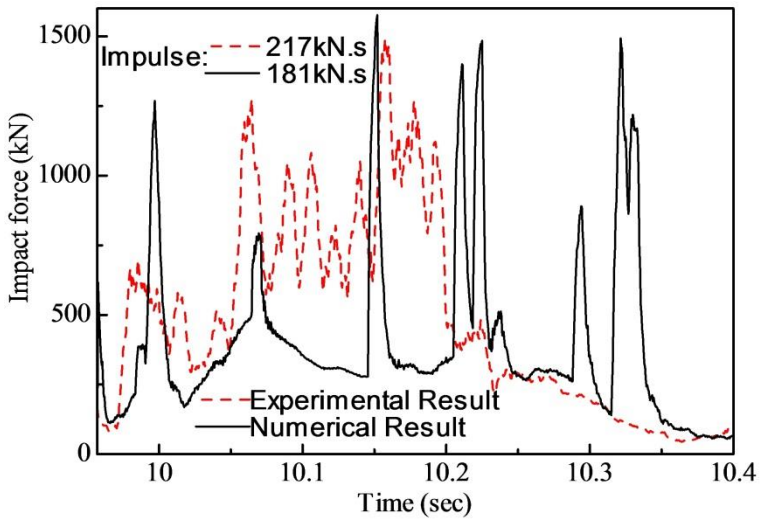


Figure 3.19 Impact force of block in Model No.2 and Test No.2

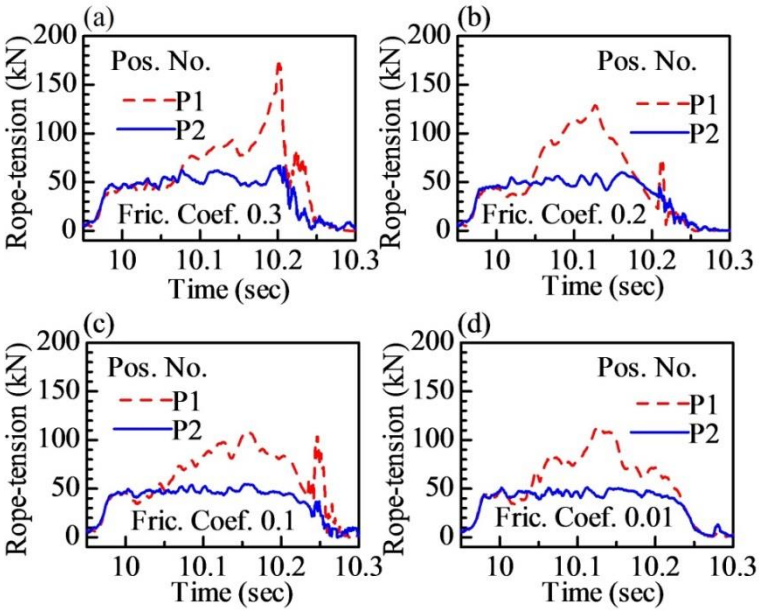


Figure 3.20 Rope tension of rope No.5 for corresponding friction coefficients

Figure 3.19 shows the impact force history of the colliding block in Test No. 2 and Model No. 2. There are obvious differences in the shape and timing of the peak value between the two curves. However, there is good agreement between the experiment and numerical analysis in terms of impulse (i.e., the time integration of the impact force) and time duration of the impact. These results demonstrate that Model No. 2 is a relevant simulation.

Figure 3.20 shows the tension of rope No. 5 measured at points P1 and P2 shown in Fig. 3.6. To examine the effects of friction between wire rope and vertical braces or intermediate posts, the friction coefficient for the contact condition in LS-DYNA was changed as 0.3, 0.2, 0.1, and 0.01 in Fig. 3.20a, 3.20b, 3.20c and 3.20d, respectively. The figure shows that (1) the rope tensions measured at P1 and P2 points were remarkably dissimilar and (2) the amplitude of the variation in rope tension along the rope line declined with a decrease in the friction coefficient. Furthermore, the rope tensions at points P1 and P2 were almost the same in the short initial period of the collision when deformation of the ropes was not great and the slipping of wire rope through an absorber has not occurred yet. However, when the ropes started slipping, the friction became available and obstructed the ropes' slipping, resulted in the raise of the rope tension in the impact

section. Therefore, evaluating the rope tension in the impact section allows consideration of the critical state of the wire rope. Moreover, although the friction coefficient was almost equal to zero in Fig. 3.20(d), there was still a difference in rope tension between P1 and P2 along the rope line. Of course, not only the friction between wire rope and vertical braces or intermediate posts but also the rope vibration due to the colliding block having many sharp edges might affected the variation in rope tension.

## 3.6 Further Numerical Analysis

It seems that the Type-B energy absorber has greater capacity for dissipating impact energy and is better able to prevent the breaking of wire ropes; however, it is difficult to carry out additional experiments to confirm this. Numerical Model No. 2 was used in further numerical analysis with the aim of gaining a deeper understanding of the structural behavior of the rock fence. A parametric study was then executed.

### 3.6.1 Further Examination of the Wire Netting and Posts

Since the damage to the wire netting was mild in both Test No. 2 and Model No. 2, the second layer of wire netting seems to be somewhat redundant. To verify this point, two different versions of Model No. 2 were created with one layer of wire netting having a 50 × 50-cell or 150 × 150-cell grid. Numerical results indicated that the rock fence could capture the RC-block in both cases, though the damage to wire netting was more severe in the latter case than in the former case. However, because of the possibility of bullet phenomenon the case of 150 × 150-cell grid will not be considered a relevant choice. This consideration should be taken into account in constructing practical rock fences.

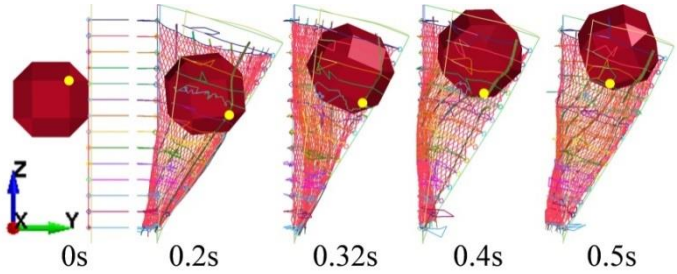


Figure 3.21 Composite picture from animation of intermediate post directly hit

Next, it is crucial whether the intermediate post would be able to sustain a direct hit by a RC-block, because this point has not been discussed in either the full-scale tests or the simulation on the rock fence. Another simulation of the impact at two-thirds height of the intermediate post in Model No. 2 was executed to verify the behavior of the post under the direct impact. Figure 3.21 shows that the post was entirely able to withstand the direct hit of the RC-block, which rolled up but did not bounce over the fence. Although local damage to a beam element under direct impact cannot be considered, this simulation result appears to be reliable because a post of concrete-filled tubular (CFT) steel is deformable and can resist a local direct hit (Maegawa et al. 1994).

### 3.6.2 Energy Absorption Capacity of the Rock Fence

The energy absorption capacity of a rock fence is defined as the maximum kinetic energy of rockfall that the rock fence can capture.

To determine the energy absorption capacity of the fence, all parameters of Model No. 2 were left unaltered, except for the magnitudes of the rotation and translation velocities. Many simulation analyses had been carried out by gradually increasing the impact energy with arithmetic progression of 50 kJ through various combinations of the two component velocities until the fence failed to capture the RC block; i.e., the block bounced over the fence without breaking the wire ropes because of the effectiveness of the absorbers. In these analyses, ratios of rotational energy to impact energy from 10% to 20% were examined according to the expected value in the practical design. Eventually, the highest energy for which the fence was able to catch the RC block was determined to be the energy absorption capacity of the fence. However, the highest energy firmly

depends on a critical value of rotation velocity; i.e., when the rotation velocity exceeds this critical value, the RC-block bounces over the fence. The lower the critical rotation velocity, the higher the energy absorption capacity, as shown in Table 3.3. Only in the case of impact energy of 926 kJ is the magnitude of the rotation velocity not critical for the fence to catch the block. To further clarify this behavior of the fence, two composite animations are shown in Figs. 3.22 and 3.23, which respectively were obtained for Model No. 2 under impact energy of 1000 kJ with rotation velocities of 16 and 18 rad/s. These figures show that the fence could capture the block having rotation and translation velocities of 16 rad/s and 17.8 m/s but not the block having rotation and translation velocities of 18 rad/s and 17.3 m/s. This result suggests that the magnitude of the rotational velocity should be considered in designing this type of fence.

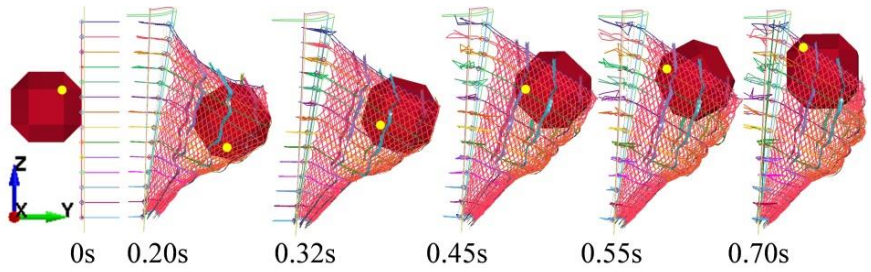


Figure 3.22 Composite picture in Model No. 2 under E (1000 kJ) and $\omega$ (16 rad./s)

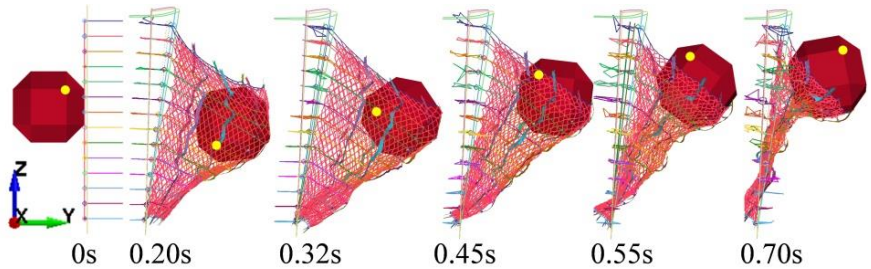


Figure 3.23 Composite picture in Model No. 2 under E (1000 kJ) and $\omega$ (18 rad./s)

Table 3.3 Critical rotation velocity for typical impact energy levels

| Impact Energy $E$ (kJ) | Critical Rotation Velocity $\omega$ (rad./s) | Ratio of Rotational Energy $Er/E$ (%) |
|---|---|---|
| 926 | Not available | |
| 1000 | 16 | 17.5 |
| 1050 | 14 | 12.7 |
| 1100 | 13 | 10.5 |

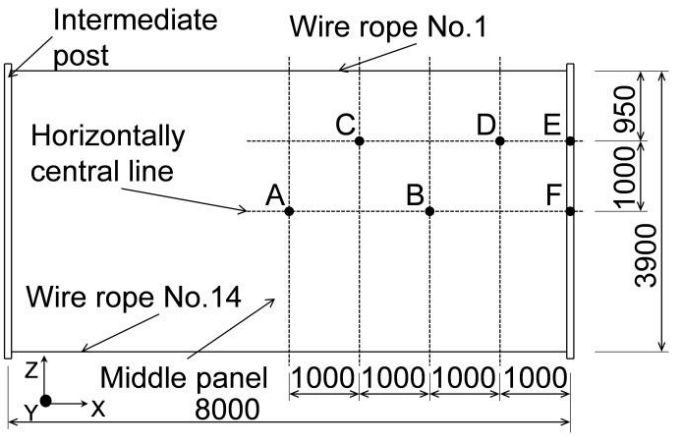


Figure 3.24 Map of impact locations (unit: mm)

Next, to survey the effect of the location of the collision point on the energy absorption capacity of the rock fence, several models were created by varying the impact position. These impact positions are indicated by the letters "A" to "F" in Fig. 3.24. Table 3.4 shows that the resistance of the fence, not being uniform, strongly depends on the impact location. The ratio of rotational energy was more than the 10% recommended by the Rockfall Mitigation Handbook (Japan Road Association 2006) in all cases, except in the case of position A, for which the magnitude of rotational velocity did not affect the energy absorption capacity of the fence. The most noticeable point here is that the impact energy absorption capacity of the fence was greater for impacts closer to the intermediate posts. For instance, the resistance of the fence corresponding to impact points B and D was higher than that for points A and C. Moreover, these results match well with those obtained by Cazzani (A Cazzani et al. 2002). In addition, the resistance of

the fence was seriously reduced for higher impact points on the wire mesh such as points C and D. However, the situation was the opposite for impact locations on the intermediate posts, in that an impact near the post base was more critical. This suggests that thorough consideration of the impact position is crucial in determining the energy absorption capacity of the fence.

Table 3.4 Energy absorption capacity of the rock fence according to six different points of impact

| Impact Location | Energy Absorption Capacity $E$ (kJ) | Critical Rotation Velocity $\omega$ (rad./s) | Ratio of Rotational Energy $Er/E$ (%) |
|---|---|---|---|
| Position A | 1400 | Not available | |
| Position B | 1550 | 19 | 15.9 |
| Position C | 450 | 10 | 15.1 |
| Position D | 700 | 12 | 14 |
| Position E | 900 | 14 | 14.9 |
| Position F | 850 | 14 | 15.7 |

## 3.7 Conclusion

In this chapter, numerical simulation using the finite element code LS-DYNA to model the rockfall collision in both Tests No. 1 and No. 2 was stated. Generally, the numerical results agree fairly well with the experimental results in terms of deformation of the whole fence, the structural behavior of each component, and the acceleration or impact force of the RC block. Furthermore, they provide further insight into the responses of individual components and the fence as a whole, particularly the effect of friction between wire ropes and intermediate posts or vertical braces on the distribution of rope tension along the rope line. Further numerical simulation has provided valuable information relating to the intensive ductility of the posts and structural behavior of wire netting under rockfall impact, leading to the possibility of reducing the wire netting from two layers to one layer or even one coarser layer with a grid of 150 × 150 cells, which would reduce costs. A thorough examination of how the position of the collision point affects

the performance of the rock fence showed that the resistance of the fence greatly depends on the impact location. The energy absorption capacity of the fence was greater for impact locations closer to the intermediate posts but seriously decreased for impact points above two thirds of the fence height. The numerical results also indicated that the magnitude of the rotational velocity of the block is an important factor determining whether the fence can catch the block in various cases of impact position. This suggests that the overall flexibility of the fence is not always sufficient to catch a block regardless of the rotational velocity. However, the ratio of the critical rotational energy for most of specific impact locations was much higher than 10%, which is the value frequently used in practice and recommended by the Rockfall Mitigation Handbook (Japan Road Association 2006).

As a final remark, it should be emphasized that the integration of full-scale tests and numerical simulation is crucial to the inspection and verification of a rock fence subjected to rockfall. First, experimental results obtained from full-scale tests provide a primary understanding of the overall performance of the fence, and in particular, they are necessary to validate adopted numerical models. Dynamic finite element analyses can then provide new insight into the response of the rock fence through iterative executions. Last but not least, numerical simulation is suitable in any parametric study and is therefore useful for designing purpose.

## 3.8 References

Cazzani A., Mongiovì L., Frenex T. (2002). Dynamic finite Element Analysis of Interceptive Devices for Falling Rocks. International Journal of Rock Mechanics and Mining Sciences 39(3): 303-321.

ETAG-027 (2008) Guideline for European Technical Approval of Falling Rock Protection Kits. European Organization for Technical Approvals (EOTA).

Grillo F., Rega G., Vestroni F. (1985). Ultimate Resistance of Structural Steel Elements for Impulsive Loads. Costruzioni Metalliche 37(4): 185-201.

Japan Road Association (2006) Rockfall Mitigation Handbook.

Maegawa K., Tomida M., Yoshida H. (1994). Impulsive Loading Tests on Concrete-Filled Tubular Steel Beams Reinforced with Tendon. Proceeding of ASCCS-4 531-534.

# Chapter 4 Prototype of a Wire-Rope Rockfall Protective Fence Developed with Three-Dimensional Numerical Modeling

## 4.1 Introduction

In the last decade, several models of fences providing protection from rockfall and having wide-ranging energy absorption capacities have been constructed in territories dominated by steep slopes and/or mountains. Buzzi (Buzzi et al. 2012) introduced rockfall barriers with a relatively low impact-energy absorption capacity of 35 kJ, and Gentilini introduced a series of falling-rock protection barriers with various energy absorption capacities (500, 3000, and 5000 kJ) (Gentilini et al. 2012; Gentilini et al. 2012).

Ordinarily, the performances of such structures are verified by conducting full-scale tests in which prototypes are subjected to the impact of a block whose mass and velocity are well known (Gottardi et al., 2010; Peila et al., 1998; Tajima et al., 2009; Arndt et al., 2009). However, because of the cost and time, full-scale tests cannot be carried out to obtain full knowledge of fence responses under various conditions. Therefore, numerical approaches firmly based on experimental data have been developed, and are able to accurately capture the complete fence response under dynamic conditions ( Cazzani et al., 2002; Dhakal et al. 2011; Volkwein 2005; Sasiharan et al. 2006).

Within this context, in previous chapters, the author introduced a particular type of rock fence, called a wire-rope rockfall protective fence (abbreviated as WRF), newly devised, and developed in Japan. Two full-scale tests followed by numerical modeling were carried out to thoroughly examine the fence response under different conditions of impact. Unfortunately, because of site conditions, the span dimensions (5, 8, and 5 m) of the tested prototype were not fully relevant to practical application. Moreover, wider post spacing would certainly result in appreciable cost benefits because of the reduction of post consumption. This

study therefore introduced a prototype of this type of fence with post spacing up to 10 m, assigned to all three modules as shown in Fig. 4.1. Additionally, previous work has indicated that a second layer of wire netting was largely redundant (Section 3.6), and consequently, only one layer of wire netting was used in the newly proposed prototype (referred to as the developed prototype in this study) to reduce cost. These alterations will affect the fence response, particularly in terms of fence elongation, post deformation, and ultimately the energy absorption capacity. These effects obviously need be investigated before using the prototype in practice. Commonly, the experimental approach of full-scale testing is considered first; however, this method is costly and unable to provide a diverse database of fence responses under various conditions. Therefore, the previous work (Chapter 3) proposed a numerical approach for the design and verification of this type of fence. This numerical approach was thoroughly assessed and validated using data of full-scale tests performed on two types of energy absorber. The numerical procedure can produce a relevant model that precisely capture the responses of different types of fence in rockfall events, and is thus a valuable design tool.

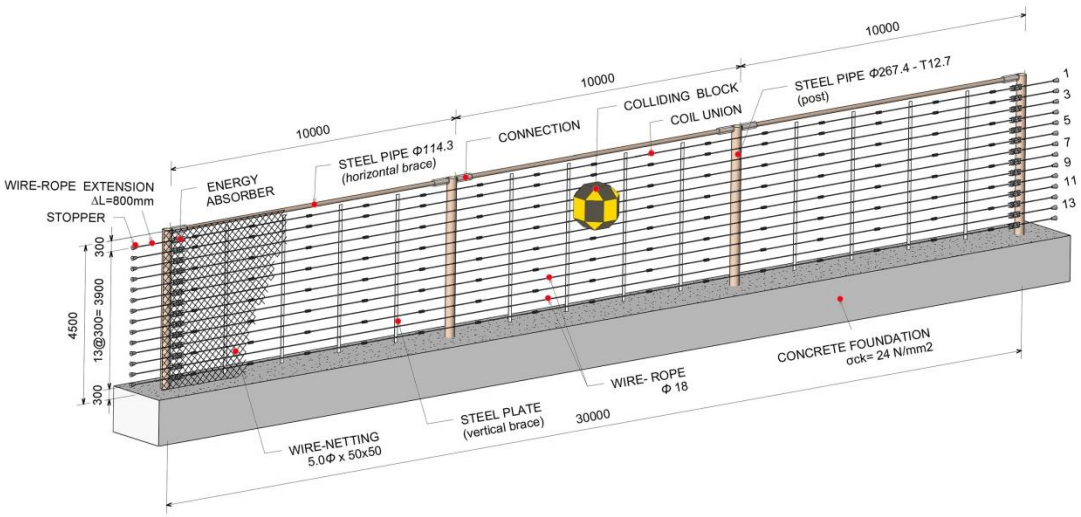


Figure 4.1 Schematic drawing of the developed prototype (unit: mm)

In this study, instead of employing an expensive experimental approach, the numerical procedure was employed to examine the new prototype of the WRF in terms of its elongation, energy absorption capacity, post deformation, and effects

of impact location and size of the colliding block. Particular attention was paid to both middle and side modules of the prototype. Detailed comparison and analysis revealed the fence performance under various dynamic conditions and the role of each constituent component of the prototype. The performance of the prototype was subsequently improved by controlling the elongation response of the prototype, which improved the energy absorption capacity. In this context, the performance of the energy absorbers was examined, helping clarify how the average friction force between the wire rope and absorber (abbreviated as AFF; refer to Section 2.3 for details) affects fence elongation. The resulting findings made it possible to improve fence resistance in a simple and efficient manner.

In addition, it would be invaluable to consider a common practical application in which the site to be protected is wide and requires at least two units of the prototype. Hence, this study also explored the performance, particularly the resistance, of a fence comprising two units of the developed prototype. The effects of the proposed method of improving the fence by changing the AFF were clarified using iterative numerical models. To the author's knowledge, this study is the first to verify the performance of such a practical form of rock fence employing a validated numerical procedure, and the study clarifies the future practical application of the prototype. Furthermore, despite the numerical procedure specifically targeting the design of the WRF, the methodologies and findings derived from this work are likely to be valuable to understanding comparable types of rock fence.

This chapter gives a brief description of the developed prototype in section 4.2, and further details are available in Section 2.2. Section 4.3 briefly summarizes the numerical procedure and closely scrutinizes the fence response to impacts targeting the middle and side modules. Section 4.4 proposes an enhancement of the prototype and presents interesting aspects fence improvement. Section 4.5 investigates the practical application of a WRF consisting of two units of the prototype. Finally, Section 4.6 is set to explore the effects of strain rate to the fence response in general.

## 4.2 Description of the Developed Prototype

The configuration of the developed prototype as depicted in Fig. 4.1 is the same as that of the previous version of the prototype, except for the post spacing and the number of wire netting layers.

The WRF has an interception structure, a support structure and connecting components (refer to Section 2.2 for additional details). The interception structure comprises 14 wire ropes, which are primarily responsible for bearing the direct block impact, and one layer of wire netting intended to support the wire ropes in arresting the block. Meanwhile, the support structure composed of concrete-filled steel posts, which are rigidly erected on a concrete foundation, firmly keeps the fence in the vertical plane without requiring lateral cables or anchors. Additionally, vertical braces, horizontal braces, steel-wire coils, and energy absorbers are connecting components.

The geometry of the prototype has post spacing of 10 m, fence nominal height of 4.2 m (defined as the initial vertical distance between the foundation top and the upper wire rope), and an interval between wire ropes of 0.3 m.

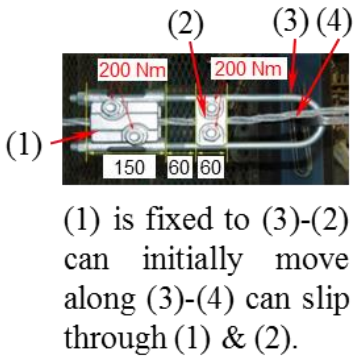


Figure 4.2 Energy absorbing device

Figure 4.2 shows functional details of the energy absorber experimentally and numerically proven to be an effective device in dissipating impact energy and preventing wire ropes from breaking (Sections 2.3 & 3.5). The efficiency of the device is attributed to the initial motion of the steel block (2) coming into contact with the steel block (1), preventing a sudden rise in rope tension at the beginning

of impact, and the relevant magnitude of the average friction force acting between the rope and two blocks (1), (2) (AFF), enabling the wire rope to slide through the device during the impact. The AFF parameter can be estimated in a laboratory dynamic test (Section 2.3) and simply altered by controlling the torque applied to the bolts connecting the steel plates in each block (1), (2).

## 4.3 Numerical Analysis of the Developed Prototype

Although only two features (the post spacing and the number of wire netting layers) were altered to create the developed prototype, there will be large inevitable and unpredictable changes to the fence's structural response. The experimental approach has routinely been applied to study such prototypes in depth, but is especially costly. This study instead employed a numerical approach proposed in the author's previous work and precisely assessed and validated using experimental data obtained in full-scale tests (Chapter 3). This inexpensive and accurate approach can precisely produce the non-linear response of a fence subjected to impacts under dynamic conditions, helping to clarify the fence's resistance in various situations of impact. Particular attention was paid to the effect of the location of impact on the fence's resistance along with its causes. In particular, to the author's knowledge, this study is the first to thoroughly examine the fence performance during an impact on the side module of the fence, in terms of fence elongation, end-post response, and impact location.

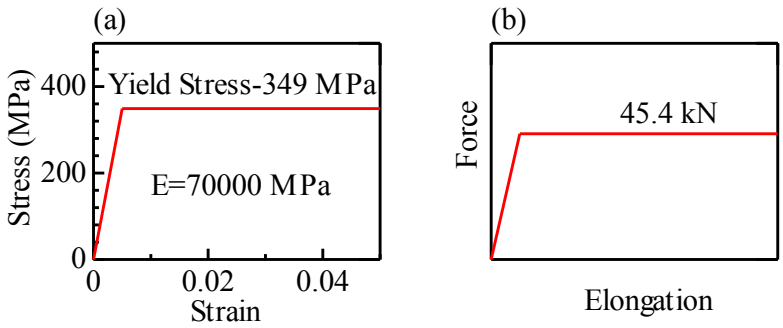


Figure 4.3 Simplification assumption of energy absorbers

To reproduce the structural behavior of the fence subjected to the direct impact of a block, numerical simulations were performed with three-dimensional dynamic finite element models using the commercially available computer program LS-DYNA. This explicit program has been proven a suitable tool for capturing dynamic and extremely rapid responses of structures to especially severe impact loads (Dhakal et al. 2011). Numerical models were based on simplifications of the material properties of fence components, such as the wire ropes, wire netting, and posts, and a simplified model of the energy absorbers with AFF of 45.4 kN as shown in Fig. 4.3. In the numerical models, the AFF could be easily altered by varying the yield stress. Similarly, to reduce computational cost, the characteristics of connections between components of the fence were also simplified (Section 3.3).

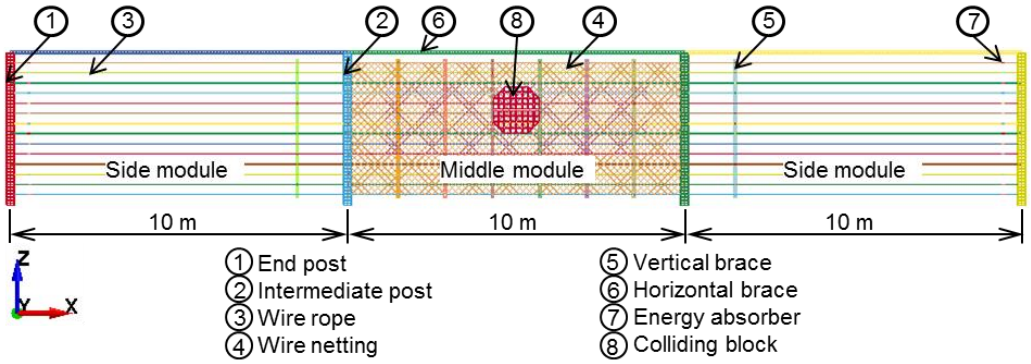


Figure 4.4 Technical sketch of the developed prototype built in LS-DYNA

Figure 4.4 built in LS-DYNA presents all constituent components of the developed prototype, whose numerical parameters are given in Table 3.1.

### 4.3.1 Numerical Analysis of the Functional Middle Module

This section presents numerical results of subsequent simulations of the functional middle module and discusses the fence response under various impact conditions relating to the impact locations as shown in Fig. 4.5 and the size of the colliding block. It is noted that the target impact locations were only at one-third and two-thirds of the fence height, which have been determined as common heights of rockfall impacts in Japan.

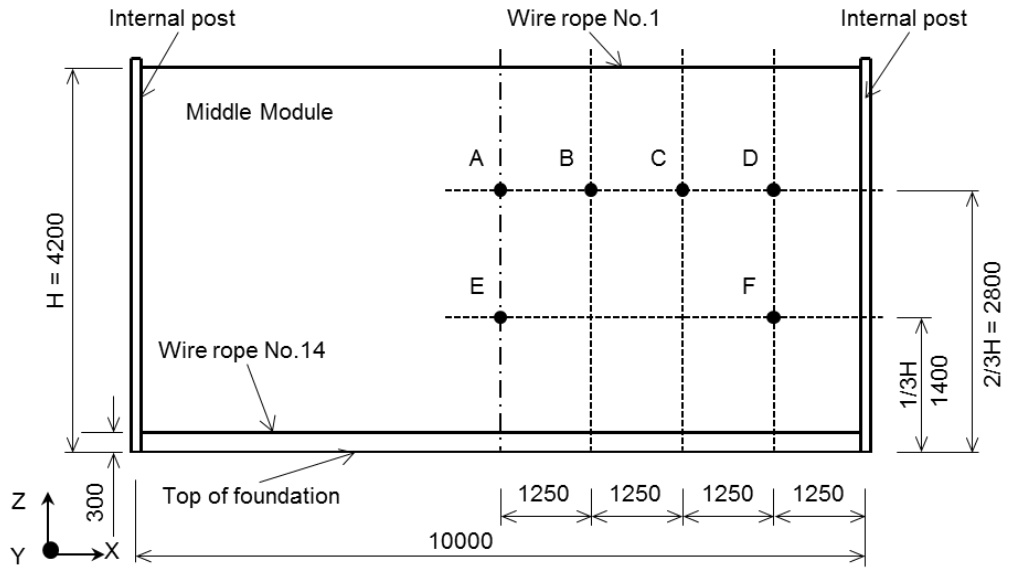


Figure 4.5 Map of impacts on the middle module (unit: mm)

Initially, to better understand how the impact location affects the resistance of the fence, it was vital to determine the fence reaction to impacts at different locations but having the same impact energy. To determine the fence reaction, impacts at two locations, points A and D as depicted in Fig. 4.5, with impact energy of 700 kJ were examined. The maximum elongation of the fence, deformation of the internal post, and roles played by wire ropes and wire netting in absorbing impact energy were examined and compared.

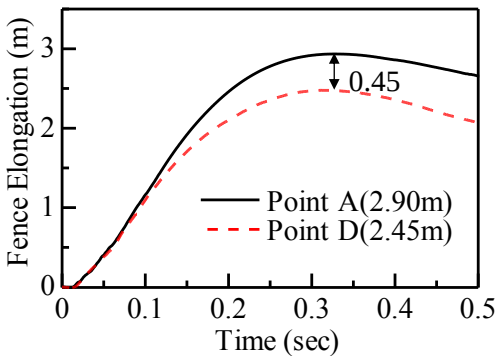


Figure 4.6 Numerical time histories of fence elongation for impacts at points A and D

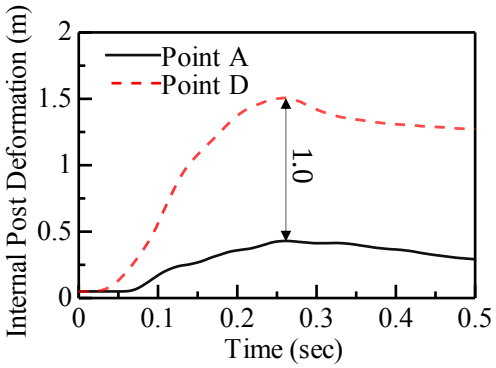


Figure 4.7 Numerical time histories of the deformation of the top of the internal post for impacts at points A and D

Figures 4.6 and 4.7 show the numerical time histories of the fence elongation and the deformation of the top of the internal post, respectively, for impacts at points A and D; the differences between the peak values were as high as 0.45 m in the fence elongation and 1.0 m in the internal-post deformation. It is thus suggested that the fence responses greatly differ in the two cases; in the case of an impact at point D, the fence elongation depended more on deformation of the internal post than elongation of wire ropes, while the opposite was found in the case of an impact at point A. This finding partly reveals the contribution of the internal post in dissipating impact energy through its remarkable deformation, especially when the impact location is quite near the internal post.

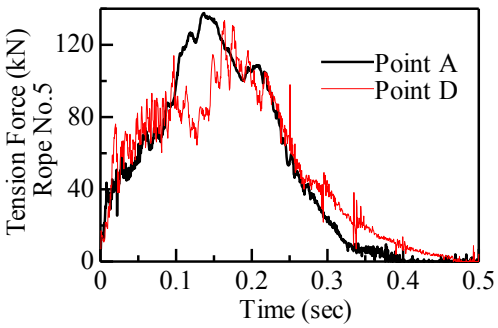


Figure 4.8 Numerical time histories of tension force of rope No. 5 for impacts at points A and D

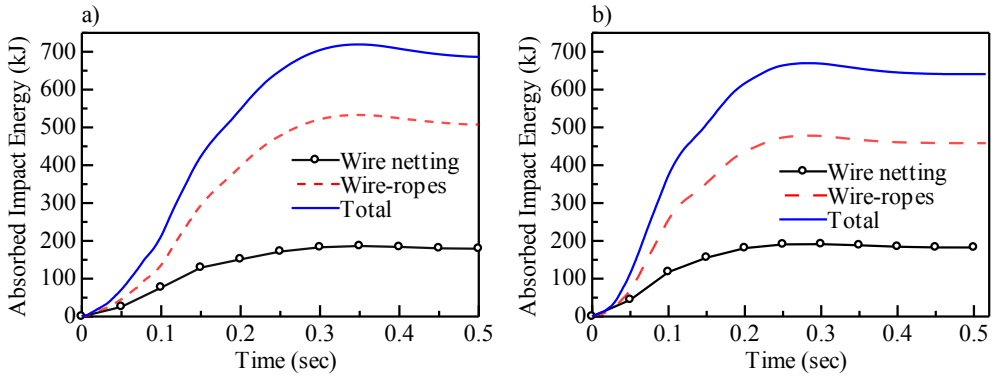


Figure 4.9 Impact energy absorbed by wire ropes and wire netting: a) impact at point A; b) impact at point D

Figure 4.8 shows that the rope tension was a little higher for an impact at point A than for an impact at point D. This result is the opposite of the fence reaction in terms of how impact energy was absorbed by the fence components, as shown in Fig. 4.9. In this case, energy absorbed by the wire ropes and netting is called contact energy, $E_{contact}$, and is incrementally updated from time *n* to *n + 1* for each contact interface as (Hallquist 2006):

$$E_{contact}^{n+1} = E_{contact}^{n} + \left[\sum_{i=1}^{nsn} \Delta F_i^{slave} \times \Delta dist_i^{slave} + \sum_{i=1}^{nmn} \Delta F_i^{master} \times \Delta dist_i^{master}\right]^{n+\frac{1}{2}} \quad (3)$$

where $nsn$ is the number of slave nodes, $nmn$ is the number of master nodes, $\Delta F_i^{slave}$ is the interface force between the *i*th slave node and contact segment, $\Delta F_i^{master}$ is the interface force between the *i*th master node and contact segment, $\Delta dist_i^{slave}$ is the incremental distance the *i*th slave node has moved during the current time step, and $\Delta dist_i^{master}$ is the incremental distance the *i*th master node has moved during the current time step.

Figure 4.9 shows that wire ropes absorbed less energy for an impact at point D. Point A is further from the internal post, and impact momentum was therefore transferred over a longer distance from the impact region to the post and dissipated by rope elongation, resulting in a severer condition for the wire ropes.

Additionally, as shown in Fig. 4.9, the portion of impact energy absorbed by wire ropes was greater for an impact at point A, while the internal post absorbed less energy, embodied by its smaller deformation as shown in Fig. 4.7. The situation for an impact at point D was the complete opposite. The significant deformation of the internal post illustrated the stronger contribution of the post in absorbing impact energy, and this appears to be a consequence of a large portion of the impact momentum being transferred by wire ropes through a shorter distance. Figure 4.9b also reveals that the total impact energy absorbed by wire ropes and wire netting was less than 700 kJ, which is the initial impact energy imparted by the colliding block, meaning that the impact energy was absorbed by the deformation of the internal post. Furthermore, Fig. 4.10 shows that for an impact at point D, the fence arrested the block quicker, again suggesting that the internal post absorbs appreciable energy through its large deformation, and seemingly resulting in a stronger fence for an impact at point D.

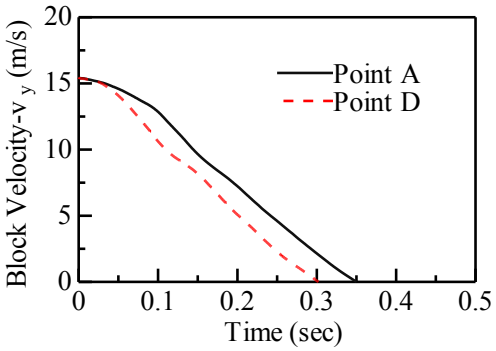


Figure 4.10 Numerical time histories of the block velocity in the Y direction for impacts at points A and D

As mentioned previously, iterative calculations were carried out to examine the effects of impact location and the size of the colliding block on the fence resistance. Impact locations were at one-third and/or two-thirds of the fence height. However, for impacts at one-third height, fewer impact locations and block sizes needed to be investigated, and the translational velocity component of the block in the Z direction was eliminated to prevent the block from landing on the ground during impact. The Rockfall Mitigation Handbook (Japan Road Association

2006) recommends that the rotational energy is consistently set as high as 10% of the total impact energy in all cases of a survey and the maximum translational velocity of the colliding block should be around 30 m/s. The minimum size of the block was therefore set as 1000 mm in the present study, because if the block is smaller than this size, the magnitude of the translational velocity is certain to exceed the limitation of 30 m/s. Thus, three blocks with maximum size D of 1400, 1200, and 1000 mm were chosen as typical samples of colliding rock blocks in the survey. Table 4.1 presents numerical results derived from the survey and relevant to the maximum capacity of energy absorption of the fence (i.e., the highest kinetic energy of a block that can be stopped by the fence) under various conditions of impact location and block size.

Table 4.1 Numerical results for fence capacity at different impact locations (points A–F of the middle module) and various block sizes. Le: maximum size D of block; Critical E: highest kinetic energy of a block that can be stopped by the fence.

| Points | Le = 1000 mm | | Le = 1200 mm | | Le = 1400 mm | |
|---|---|---|---|---|---|---|
| | Critical E (kJ) | $v_y$ (m/s) | Critical E (kJ) | $v_y$ (m/s) | Critical E (kJ) | $v_y$ (m/s) |
| Point A | 700 | 25.9 | 720 | 19.9 | 800 | 16.5 |
| Point B | 720 | 26.3 | 750 | 20.3 | 820 | 16.7 |
| Point C | 750 | 26.8 | 850 | 21.6 | 950 | 18.0 |
| Point D | 950 | 30.9 | 970 | 23.1 | 1100 | 18.9 |
| Point E | 400 | 19.7 | 400 | 14.9 | 400 | 11.6 |
| Point F | 800 | 27.8 | 900 | 22.4 | 1000 | 18.6 |

For all dimensions of the block, the fence resistance gradually increased along the line of impact points from A through D; i.e., the resistance of the fence was

maximum for an impact at point D. This trend was unaffected by the block size. This is consistent with this previous finding that the nearer the impact is to the internal post, the stronger the fence response. The table also shows that the fence resistance strongly depended on the size of the block, in that it gradually weakened as the block size decreased. This relation is simply explained by the fact that for the same impact energy, the smaller the block, and the greater the block velocity, especially the rotational velocity component, which facilitates the block to roll over the fence in cases where the impact is targeted at two-thirds of the fence height. For an impact at point E, there was no dependence on the block size because the dominant elongation of wire ropes led to large deformation of the fence and the block easily rolled through the bottom of the fence without rope breakage. Additionally, it is likely that the decrease in fence resistance in this case is a predictable outcome of small deformation of the internal post. The above findings firmly suggest that the block size should be seriously considered in determining the fence resistance in general.

Interestingly, it is noted that in almost all cases of the fence failing to catch the block, the block rolled over or under the fence without any breakage of wire ropes, which is certainly attributable to critical elongation of the fence. This means that an appropriate critical elongation is a possible key feature with which to enhance the fence performance.

### 4.3.2 Numerical Analysis of the Functional Side Module

This section explores the performance of the fence with impacts on the side module. Similar to the analysis of the middle module, the fence response to impacts at points H and I as indicated in Fig. 4.11 was investigated in the terms of fence elongation, displacement of the top of the end post, bending moment acting on the base of the end post, impact energy absorbed by wire ropes and wire netting, and velocity of the block.

Figure 4.12 shows the numerical time histories of the fence elongation for impacts at points H and I. The difference in peak values of 0.4 m was approximately the same as that (0.45 m; Fig. 4.6) in the case of the middle module. However, the trends of the fence elongation history were rather different between the two cases examined for the side module, particularly at the beginning of impact. This

is explained by the greater effect of energy absorbers, which were immediately next to the impact location, on the fence response to an impact at point I. In other words, after significant sliding of the wire ropes through absorbers resulting in larger elongation of the fence at the beginning of impact, the stoppers hit the absorbers and slowed the lengthening of the wire ropes, causing the fence elongation to become less severe as shown in Fig. 4.12. Another reason is the difference in the end-post deformation between the two cases as depicted in Fig. 4.13.

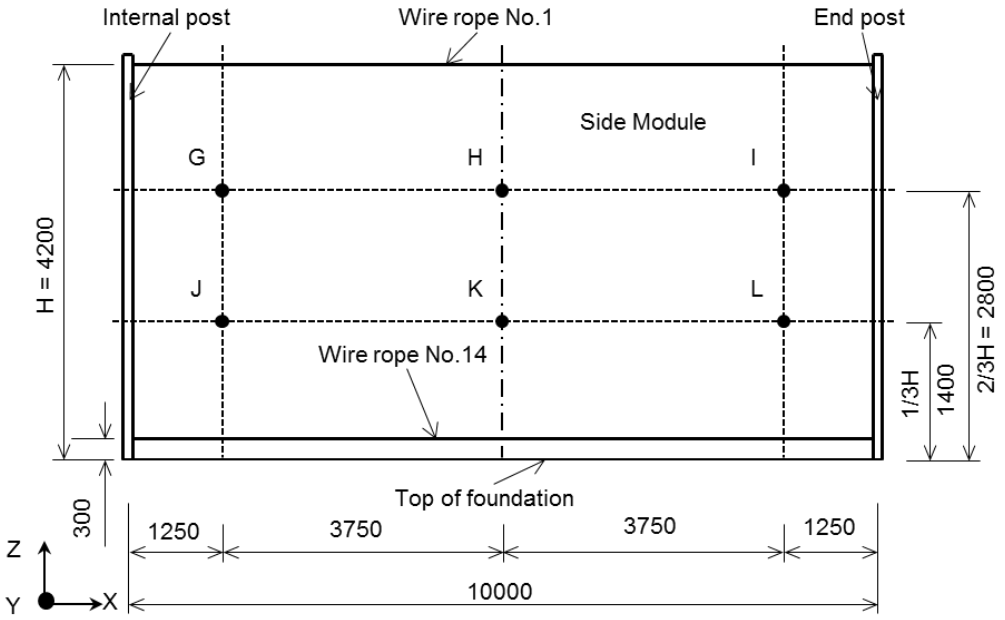


Figure 4.11 Map of impacts on the side module (unit: mm)

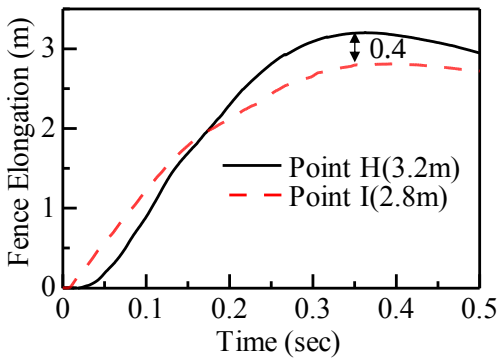


Figure 4.12 Numerical time histories of fence elongation for impacts at points H and I

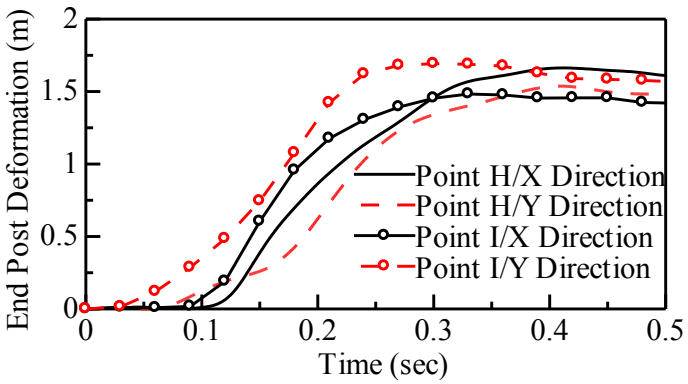


Figure 4.13 Numerical histories of deformation of the top of the end post for impacts at points H and I

Figure 4.13 illustrates the displacements of the top of the end post in both X and Y directions for impacts at points H and I. For impacts at both points, the end post deformation was relatively homological in the X and Y directions, and severe as the peak values exceeded 1.5 m, resulting in a critical moment (over 700 kNm) measured at the base of the end post as shown in Fig. 4.14. However, because the impact at point I was immediately next to the end post (i.e., much more impact energy was transferred to the end post, resulting in severer deformation of the end post as shown in Fig. 4.13), the proportion of impact energy absorbed by wire ropes and wire netting differed between the two cases as shown in Fig. 4.15.

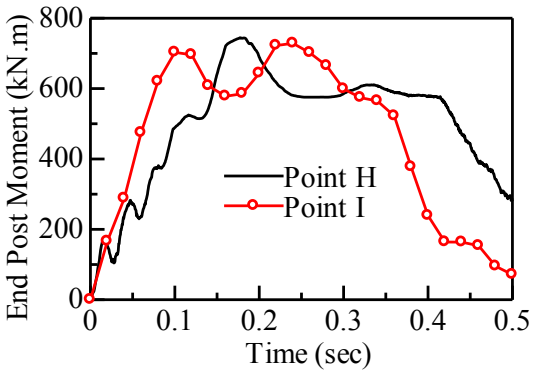


Figure 4.14 Numerical histories of the base moment of the end post for impacts at points H and I

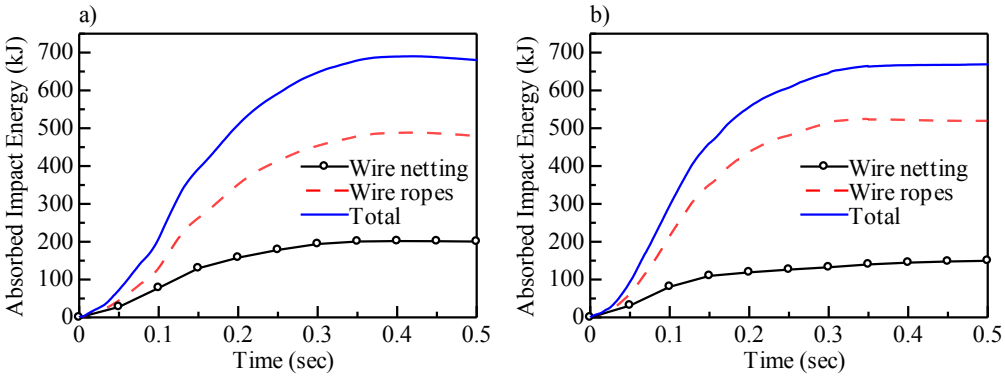


Figure 4.15 Impact energy absorbed by wire ropes and wire netting: a) impact at point H; b) impact at point I

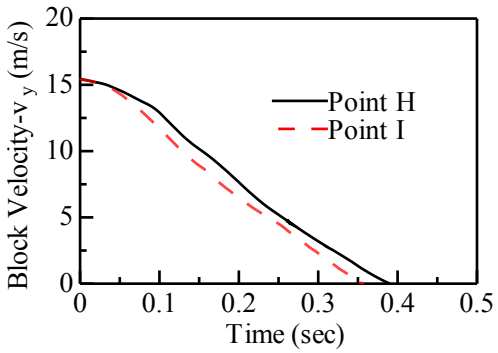


Figure 4.16 Numerical time histories of the block velocity in the Y direction for impacts at points H and I.

Figure 4.15 shows that although proportions of impact energy absorbed by wire ropes and wire netting varied in the two cases, the totals of absorbed energy were a little less than the initial impact energy of 700 kJ in both cases, and similar to the energy absorbed during the impact at point D of the middle module. These results again assert the contribution of the sizable deformation of posts in dissipating energy.

The results presented in Figs. 4.13, 4.15, and 4.16 reveal that the more severely the end post is deformed, the greater the contribution of the end post in dissipating impact energy. Furthermore, comparison of Figs. 4.10 and 4.16 shows that the fence took longer to catch the block in the case of an impact on the end module. Additionally, in comparison with the case for impacts at points A and D of

the middle module, the difference in the fence response between impacts at points H and I was small. This was further evidenced by numerical results obtained in a series of simulations aimed at surveying the fence resistance for various impact locations as shown in Table 4.2. Indeed, the fence resistance remained unchanged at 700 kJ for impacts at points H, I, K, and L and the resistance to impacts on the side module was less than that to impacts on the middle module. This is attributable to the immense deformation of the end post, especially in the X direction. With impact energy of 800 kJ targeted at point H, the end post broke at its base as depicted in Fig. 4.17 and the block rolled over the fence. The post breaks in this case because the effective plastic strain at its base exceeds the critical magnitude of 0.35 as a failure condition, which is the average value of effective plastic strain Ip1–Ip4 (Ip1–Ip4 are four integral points of a beam element). Effective plastic strain can be calculated as (Hallquist 2006):

$$\varepsilon_p = \varepsilon - \left(\frac{\sigma}{E}\right) \tag{4}$$

Where $\varepsilon$ is total strain, $\varepsilon$ is true stress, and E is Young's modulus.

When the impact energy was scaled down to 750 kJ, the end post did not break but the fence still did not stop the block. However, the fence had higher strength for impacts at points G and J, which are quite far from the end post; the fence response in these cases was not dominated by huge deformation of the end post. Instead, these points, like points D and F, are immediately next to the internal post; hence, the fence response can be explained by the contribution of the internal post in dissipating impact energy as discussed in the previous section.

Table 4.2 Numerical results of the fence resistance for different impact locations of the side module and block size

| Point | H | I | K | L | G | J |
|---|---|---|---|---|---|---|
| Critical E (kJ) | 700 | 700 | 700 | 700 | 850 | 1200 |
| $v_y$ (m/s) | 15.4 | 15.4 | 15.4 | 15.4 | 17.0 | 20.3 |

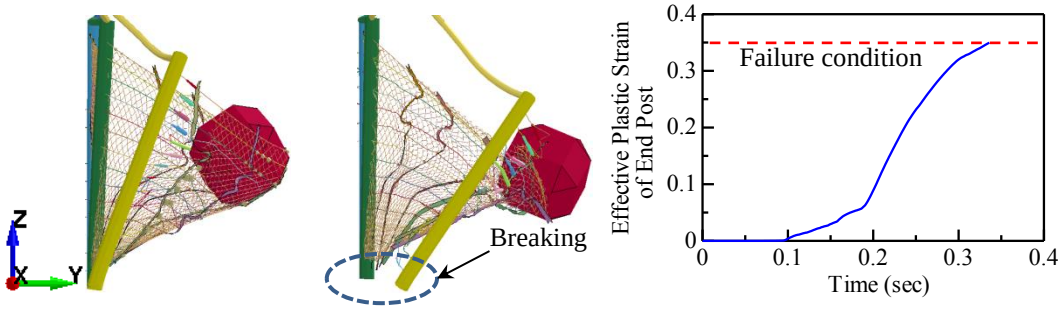


Figure 4.17 Breaking of the end post for an impact at point H of the side module with energy of 800 kJ

## 4.4 Enhancements of the Developed Prototype

As found in the previous sections, for impacts at two-thirds of the fence height, the fence failed to catch the block because the block rolled over the top of the fence as the result of a significant reduction in the fence's residual height owing to the fence's large elongation. Therefore, lessening the fence elongation is important to enhancing the fence's effectiveness. In an effort to reduce the elongation, numerical simulations of an impact at point A of the middle module with impact energy of 800 kJ and various AFF parameters of the absorber were carried out to explore the relationship between the fence elongation and AFF parameter.

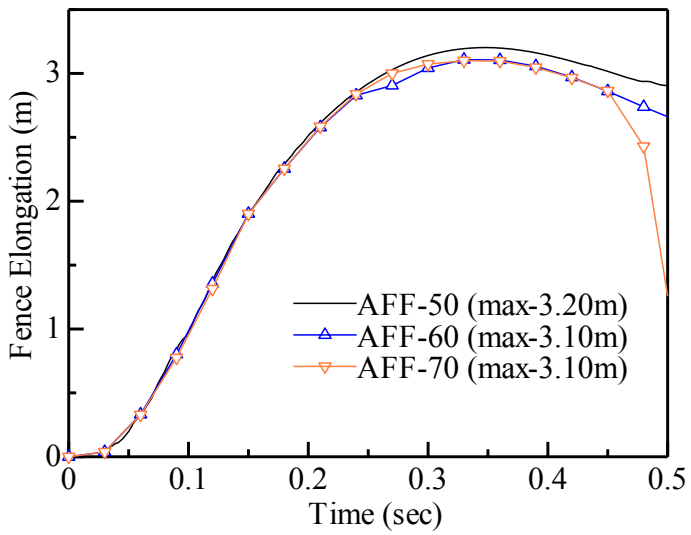


Figure 4.18 Relationship between the AFF of energy absorbers and fence elongation

Figure 4.18 shows the interesting result that the fence elongation was independent of the AFF parameter at the beginning of impact; i.e., the absorbers had not yet come into effect, and the fence elongation was initially attributed to elongation of the wire ropes and deformation of the post. When the absorbers started to come in operation, the fence elongation slightly reduced as the AFF parameter increased from 50 to 60 kN. However, it is surprising that the fence elongation remained unchanged as the AFF parameter increased from 60 to 70 kN; it is likely that at energy of 800 kJ, an AFF of 60 kN is a threshold at which the absorbers still affect the fence elongation. Moreover, according to a preliminary test of the energy absorber, the peak friction force acting between the wire rope and absorber was probably three times the AFF (Section 2.3.1); therefore, an AFF of 70 kN is inappropriate because the critical strength of wire ropes is 180 kN. Hence, an AFF of 60 kN both reduces the fence elongation and prevents wire ropes from breaking. With an AFF of 60 kN, the fence resistance for an impact at point A of the middle module increased to 950 kJ from an original value of 800 kJ corresponding to an AFF of 45 kN, which is a 19% increase, as evidently shown in Fig. 4.19.

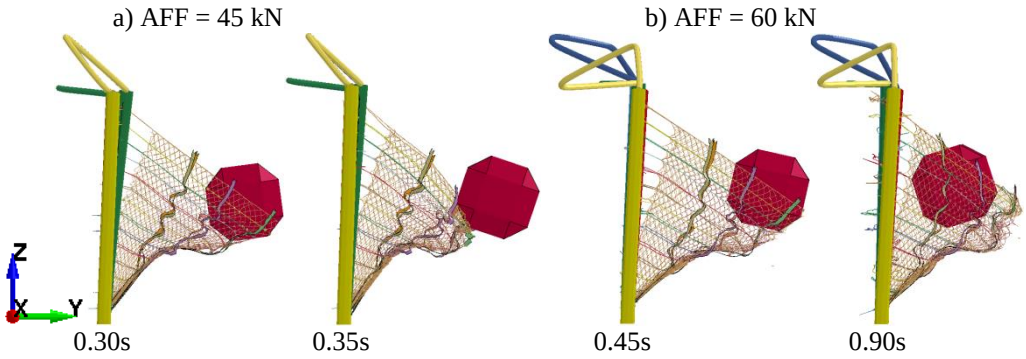


Figure 4.19 Animation of the impact at point A of the middle module with the same energy of 950 kJ but different AFFs: a) AFF of 45 kN ; b) AFF of 60 kN

More interestingly, the numerical result in Fig. 4.20 shows that the energy absorption capacity of the fence for an impact at point E of the middle module surprisingly increased from 400 for an AFF of 45 kN to 750 kN for an AFF of 60 kN, which is an increase of 87%. The improvement is considerable and suggests

that the fence resistance is especially sensitive to the elongation of the wire ropes in this case.

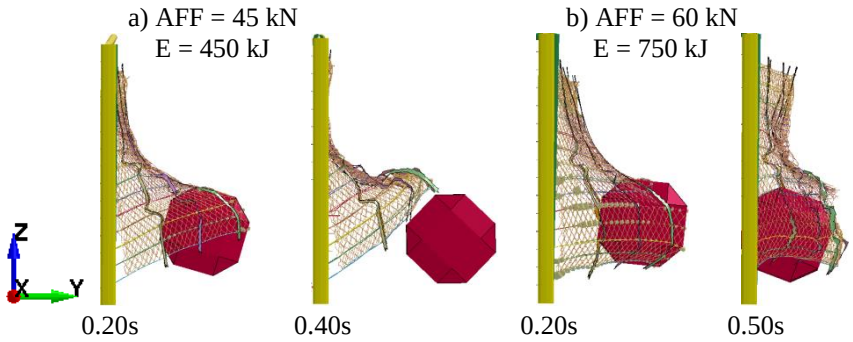


Figure 4.20 Animation of the impact at point E of the middle module at impact energies of 450 kJ (a) and 750 kJ (b)

The results show that the fence can be considerably strengthened in a simple but effective manner by changing the AFF parameter through altering the torque of the M20 bolts (Section 2.2.1).

## 4.5 Practical Application of the Developed Prototype

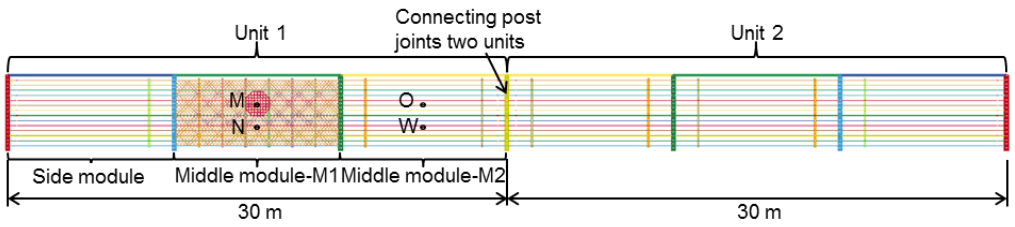


Figure 4.21 Technical sketch of the model of two fence units erected side by side

In practice, the length of a site that needs to be protected commonly exceeds the prototype length (30 m). In this case, at least two units of the developed prototype must be erected side by side as shown in Fig. 4.21, and the performance of the fence as a whole would change considerably; it is thus important to investigate this case. In particular, the energy absorption capacity of the whole fence for impact locations on modules M1 and M2 should be comprehensively explored to assist the practical application of the prototype.

To carry out such analysis, iterative numerical models were calculated, and results for the energy absorption capacity of modules M1 and M2 as constituent parts of the whole fence, obtained using the models, are presented in Table 4.3. For brevity, only two impact locations are considered for each module, one at one-third height (points N and W) and the other at two-thirds height (points M and O) of the fence at the center of the horizontal span, as indicated in Fig. 24. Specifically, points M, O, N, and W in Fig. 4.21 correspond to points A, I, E, and L, respectively, in Figs. 4.5 and 4.11.

Table 4.3 Energy absorption capacity of a fence composed of two units of the developed prototype.

| Module M1 | | | Module M2 | |
|---|---|---|---|---|
| Point | Critical E (kJ) | | Point | Critical E |
| | AFF=45 kN | AFF=60 kN | | (kJ) |
| M | 1100 | 1200 | O | 950 |
| N | 500 | 750 | W | 850 |

The numerical data summarized in Table 4.3 show a great increase in the fence resistance when two units of the prototype are placed side by side. Specifically, the increments in fence resistance were approximately 37% and 36% for impacts at points M and O, respectively, with respect to the resistance of a single unit. The corresponding figures for impacts at points N and W were 25% and 21%, respectively. Indeed, the improvement of the fence in this situation is impressive, and much greater than that in the case of altering the AFF parameter as previously mentioned. This can be attributed to the reduced deformation of the connecting post constrained by the second unit, resulting in a remarkable decrease in overall fence elongation, as seen by comparing Fig. 4.22 with Figs. 4.6 and 4.12.

In addition, Fig. 4.23 provides evidence that the connecting post was negligibly deformed in the X direction for impacts at points M and O, while the end post was severely deformed in the case that one prototype works alone.

Next, the enhancement approach of altering the AFF (from 45 to 60 kN) was applied to the joined fence units. The fence capacity increases considerably, as expected. The energy absorption capacity of the fence increased to 1200 and 750 kJ for impacts at points M and N, respectively. Similar to the case of one unit, the increase of fence capacity for an impact at point N was larger than that for an impact at point M when the AFF is changed.

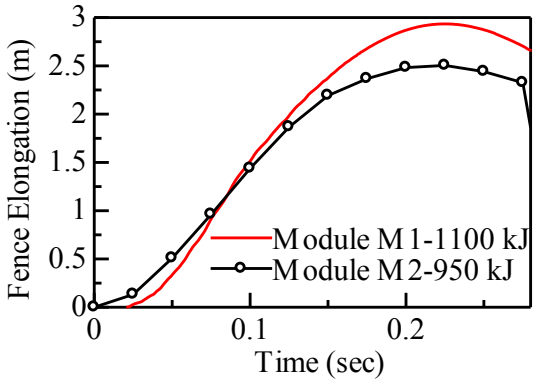


Figure 4.22 Numerical histories of the fence elongation in cases 1 and 2

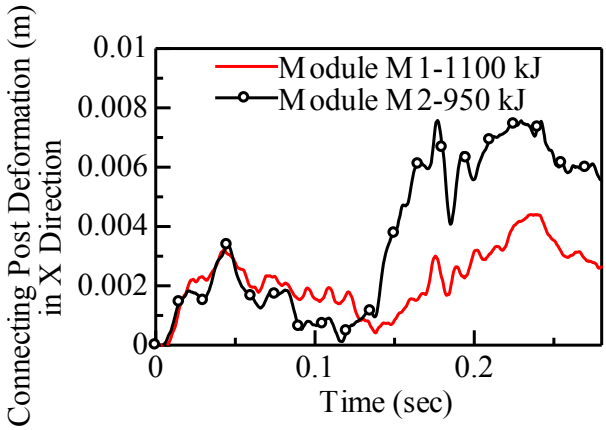


Figure 4.23 Numerical histories of the connecting post deformation in the X direction in cases 1 and 2

## 4.6 Effects of Strain Rate

Commonly the speed of rockfall is not at high degree comparing with projectile as well as blasting, however, this study also explores the effects of strain rate to the fence response in general. Strain rate is accounted for using the Cowper and Symonds model that scales the yield stress with the factor:

$$1 + \left(\frac{\dot{\varepsilon}}{C}\right)^{1/P}$$

Where $\dot{\varepsilon}$ is strain rate; C and P are strain rate parameters. I assumed C being 40 and P being 5 to measure strain rate of posts and wire ropes for impact at point A. Relevant results are shown in Fig. 4.24

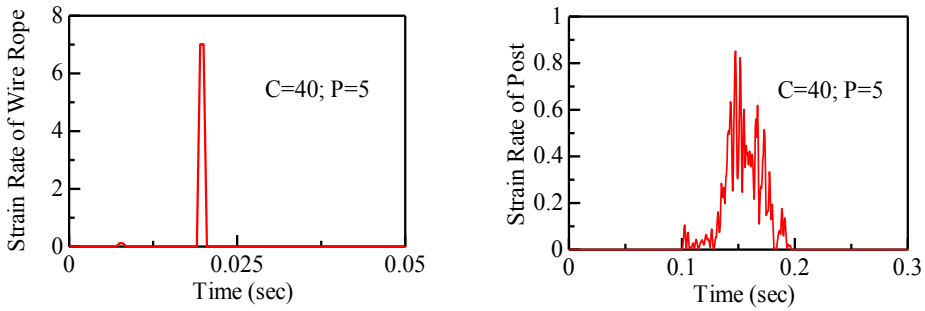


Figure 4.24 Strain rate: a) Wire ropes and b) Posts

Numerical results disclose that the deformation of internal post decreased considerably under effects of strain rate, resulting in reduced elongation of the fence as a whole as illustrated in Fig. 4.25

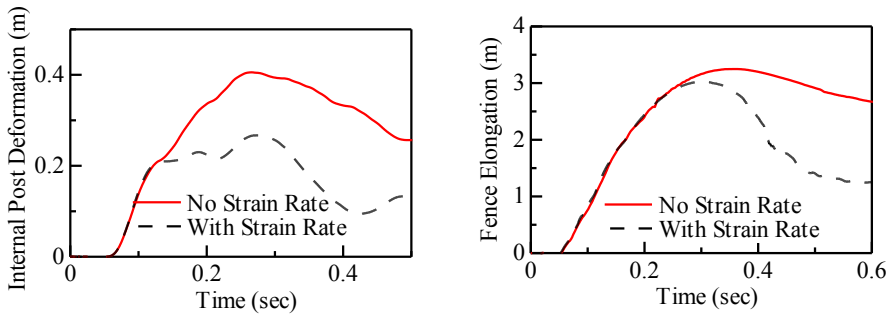


Figure 4.25 Effects of strain rate to the fence response in terms of post deformation and fence elongation

As a result, the amount of impact energy absorbed by the fence was recognized to slightly drop as shown in Fig. 4.26, causing the fence failed to catch the block. However, it is noted that these finding results just explore the effects of strain rate to the fence response in general, its accuracy strongly depends on the relevance of strain rate parameters C and P, and more importantly, the real post is CFT structure, hence effects of strain rate to CFT may be different.

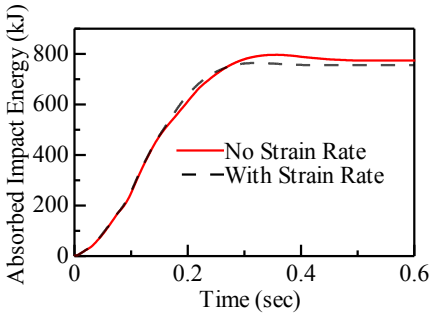


Figure 4.26 Fence response to strain rate in term of absorbed impact energy

## 4.7 Conclusion

On the basis of findings of previous work (Chapters 2 & 3), a newly developed prototype of the WRF was introduced for mainly cost reasons, and the prototype was investigated employing a numerical procedure that has been validated with experimental data obtained in full-scale tests. In this study, the non-linear responses of functional middle and side modules, as constituent parts of the prototype, to the impact of a block having varying mass and velocity were examined in detail. The results provide insight into how the fence reacts to impacts under different conditions of impact location and block size. The role of each key component of the prototype was thus revealed. Of particular interest was the contribution of posts in dissipating energy.

From the knowledge obtained about this prototype and its resistance limitations, an approach for improving fence performance was suggested. This especially simple approach of altering the AFF parameter of energy absorbers was numerically demonstrated to be effective. The energy absorption capacity of the fence increased at least ~20% (150 kJ), matching the capacity of other types of rock fence (Dhakal et al. 2012). The AFF parameter could be easily changed by controlling the torque of M20 bolts connecting components of the energy absorber.

Furthermore, the study considered the common situation in which a fence comprising two units of the prototype is required to protect a wide area. Employing the same numerical procedure used earlier in the study, iterative models were an-

alyzed to clarify the performance of this fence. In addition, the two-unit fence was found to be strengthened using the proposed enhancement approach, again asserting the effectiveness of the approach for the developed prototype.

Finally, although the response of the developed prototype was only analyzed employing a numerical approach, the results obtained are valuable for the practical application of this prototype and for further research on this type of rock fence or similar types developed in the future.

## 4.8 References


Cazzani A., Mongiovì L., Frenex T. (2002). Dynamic Finite Element Analysis of Interceptive Devices for Falling Rocks. International Journal of Rock Mechanics and Mining Sciences 39(3): 303-321.

Arndt B., Ortyz T., Keither Turner A. (2009). Colorado ' s Full-Scale Field Testing of Rockfall Attenuator Systems. Transportation Research Board of the National Academies.

Buzzi O., Spadari M., Giacomini A., Fityus S., and Sloan S. W. (2012). Experimental Testing of Rockfall Barriers Designed for the Low Range of Impact Energy. Rock Mechanics and Rock Engineering

Dhakal S., Bhandary N. P., Yatabe R., Kinoshita N. (2011). Experimental, Numerical and Analytical Modelling of a Newly Developed Rockfall Protective Cable-net Structure. Natural Hazards and Earth System Science 11(12): 3197–3212. http://www.nat-hazards-earth-syst-sci.net/11/3197/2011/

—— (2012) Numerical and Analytical Investigation Towards Performance Enhancement of a Newly Developed Rockfall Protective Cable-Net Structure. Natural Hazards and Earth System Science 12(4): 1135–1149. http://www.nat-hazards-earth-syst-sci.net/12/1135/2012/

Gentilini C., Gottardi G., Govoni L., Mentani A., Ubertini F. (2012). Design of Falling Rock Protection Barriers Using Numerical Models. Engineering Structures. http://linkinghub.elsevier.com/retrieve/pii/S0141029612003690

Gentilini C., L. Govoni, S. de Miranda, Gottardi G., and Ubertini F. (2012). Three-Dimensional Numerical Modelling of Falling Rock Protection Barriers. Computers and Geotechnics 44: 58–72.

Gottardi G., Govoni L. (2010). Full-scale Modelling of Falling Rock Protection Barriers. Rock Mechanics and Rock Engineering 43(3): 261–274.

Hallquist, John O. (2006). LS-DYNA Theory Manual. Livermore Software Technology Corporation.

Japan Road Association (2006). Rockfall Mitigation Handbook

Peila D., S. Pelizza, and F. Sassudelli (1998). Evaluation of Behaviour of Rockfall Restraining Nets by Full Scale Tests. Rock Mechanics and Rock Engineering 31(1): 1–24.

Sasiharan N., B. Muhunthan, T. Badger, Shu S., and Carradine D. (2006). Numerical Analysis of The Performance of Wire Mesh And Cable Net Rockfall Protection Systems. Engineering Geology 88(1-2): 121–132.

Tajima T., Maegawa K. (2009). Evaluation of Pocket-type Rock Net by Full Scale Tests. Proc. of 33rd IABSE.

Volkwein, A. (2005). Numerical Simulation of Flexible Rockfall Protection Systems. Computing in Civil Engineering 179: 122–122.

# Chapter 5 Conclusion

This study focused on development of a newly flexible fence as one of the most effective protection approach against rockfall events having been becoming an increasing threat to human as well as transportation in mountainous areas all round the world. Distinguished from other flexible fences having been recently developed in Europe, the fence is able to vertically stand by itself without lateral guy cables and anchors. This characteristic makes the fence more suited to narrow protection sites, which are commonly seen in Japan. Especially, a new type of energy absorbing device mounted on the wire-ropes was shown to be especially effective in preventing the wire-ropes from breaking. Furthermore, as a key support structure in the fence system, posts made of concrete-filled steel tubes (CFT) help enhance the fence resistance considerably, particularly in the sense of rock blocks directly strike the post.

In the way to deeply reach the nonlinear responses of the fence against rockfall, both approaches of full-scale tests and numerical simulation were conducted successfully. In particular, full-scale tests brought the most real behavior of the fence during rockfall impact, allowing access the actual way of how the fence would response against real rockfalls. A site of natural steep slope located at a mountainous area in Japan was chosen to carry out full-scale tests. The test preparation having to meet Japan standard to ensure safety during testing was performed carefully. The fence erected at the slope base was exposed to impact of an RC block falling and rolling down a natural steep slope. To obtain more detailed results from the tests such as the acceleration or impact force between the RC block colliding and the fence, a specialized measurement control system able to synchronize all measuring instruments was devised and employed. Two tests having different shock absorbers were carried out and the RC block was successfully captured in both tests with the impact energy approximately estimated as high as 900 kJ, which is lower than that of 1300 kJ expected for the site conditions (Japan Road Association 2006). However, there was a noticeable point that the rotational energy was 17% to 20% of the total impact energy, which is much more than the value of 10% recommended by the Rockfall Mitigation Handbook

(Japan Road Association 2006). This point states the complexity of rockfall mechanic prediction. Despite the higher rotational energy, because of the flexibility of the fence structure the RC block did not bounce over the fence in either test, even though the impact locations were likely at two-thirds of the fence height where the fence resistance often decreases significantly. More importantly, the residual deformation of the fence after impact was about 1000 mm, making the fence suitable to be installed just aside roads, where very little space exists. This result well meets the design scope of the fence as mentioned previously.

Two types of energy absorber, namely Type-A and Type-B, examined in laboratory pre-tests were assembled for the rock fences in the full-scale tests to confirm their energy-dissipation functions. The Type-B was found to be effective in preventing wire-rope breakage and in dissipating the impact energy of rockfall and it thus considerably enhanced the impact energy absorption capacity of the fence. As mentioned in Chapter 2, the solely difference to distinguish two types of energy absorber is the interval of 60 mm between steel blocks as key components of the absorber, leading to dissimilarity in the AFF parameter. Ultimately their functional efficiency differed surprisingly. This finding is recognized as the most beneficial point because there is no difference in cost between Type-A and Type-B of absorber.

As a powerful supplement to full-scale tests, numerical simulation using the commercial available program, finite element code LS-DYNA, was executed to reproduce the rockfall collision in both Tests No. 1 and No. 2. In general, the numerical results meet fairly well with the experimental results in terms of deformation of the whole fence, the structural performance of each component, and the acceleration or impact force of the RC block. In addition, they provide further insights into the non-linear responses of individual components and the fence as a whole under dynamic conditions, particularly the effect of friction between wire ropes and intermediate posts or vertical braces on the distribution of rope tension along the rope line. Especially, further numerical simulation has been successfully implemented to provide valuable information relating to the intensive ductility of the posts and structural behavior of wire netting under rockfall impact, leading to the possibility of reducing the wire netting from two layers to one layer or

even one coarser layer with a grid of 150 × 150 cells, which would reduce costs. A thorough examination of how the location of the collision point affects the performance of the rock fence showed that the resistance of the fence greatly depends on the impact location. The energy absorption capacity of the fence was greater for impact locations closer to the intermediate posts but seriously decreased for impact points above two thirds of the fence height. The numerical results also indicated that the magnitude of the rotational velocity of the block is an important factor determining whether the fence can catch the block in various cases of impact location. This suggests that the overall flexibility of the fence is not always sufficient to catch a block regardless of the rotational velocity. However, the ratio of the critical rotational energy for most of specific impact locations was much higher than 10%, which is the value frequently used in practice and recommended by the Rockfall Mitigation Handbook (Japan Road Association 2006). In general, although there are still differences between numerical results and those obtained from full-scale test, particularly in terms of rope tension as well as the number of broken wire-rope, the accuracy of the numerical procedure in reproducing the fence performance under various dynamic conditions is indisputable.

On the basis of findings achieved from both full-scale tests and numerical simulation, a newly developed prototype of the wire-rope rock fence was introduced for mainly cost reasons, and the prototype was investigated employing above numerical procedure that has been validated with experimental data obtained in full-scale tests. In particular, the non-linear responses of functional middle and side modules, as constituent parts of the prototype, to the impact of a block having varying mass and velocity were examined in detail. The results disclose in more details how the fence reacts to impacts under various conditions of impact location and block size, and behind reasons were also discussed through numerical analysis. The role of each key component of the prototype was thus revealed comprehensively. Of particular interest was the contribution of posts in dissipating energy.

The thorough numerical examination on the fence helped find out its resistance limitations, an approach of fence performance improvement was therefore sug-

gested. This especially simple approach of altering the AFF parameter of energy absorbers was numerically demonstrated to be highly effective. The energy absorption capacity of the fence increased at least ~20% (150 kJ). The AFF parameter could be easily changed by controlling the torque of M20 bolts connecting components of the energy absorber.

In addition, the common situation in which a fence comprising two units of the prototype was numerically considered. This practical application is often required to protect a wide area, frequently seen along vehicle road in Japan. Based on the same numerical procedure, iterative models were analyzed to clarify the performance of this application. Furthermore, the two-unit fence was found to be strengthened using the proposed enhancement approach, again asserting the effectiveness of the enhancement approach for the developed prototype. Although the response of the developed prototype was only analyzed employing a numerical approach, the results obtained are valuable for the practical application of this prototype and for further research on this type of rock fence or similar types developed in the future.

As a final remark, the emphasis here is that to accurately investigate and verify a rock fence subjected to rockfall, the integration of full-scale tests and numerical simulation is the most relevant approach so far. First, experimental results obtained from full-scale tests allow reaching a primary understanding of the overall performance of the fence as a whole, and in particular, they are the most trusted database to validate adopted numerical models. Then dynamic finite element analyses can be recognized as a powerful tool to provide new insights into the response of the rock fence as a whole or each constitutive component through iterative executions. In particular, this numerical tool can produce the fence response to rockfall under various conditions that is impossible to do in site test. Last but not least, numerical simulation is suited to any parametric study and is therefore useful for design or redesign work of similar type of rock fence.